SEDIMENTOLOGY the journal of the International Association of Sedimentologists

Sedimentology (2011) **58,** 1737–1761 doi: 10.1111/j.1365-3091.2011.01237.x

The sedimentary response to a pioneer geo-engineering project: Tracking the Kander River deviation in the sediments of Lake Thun (Switzerland)

STEFANIE B. WIRTH*, STÉPHANIE GIRARDCLOS*[1], CHRISTIAN RELLSTAB†‡[2] and FLAVIO S. ANSELMETTI§

**Geological Institute, ETH Zürich, 8092 Zürich, Switzerland (E-mail: stefanie.wirth@erdw.ethz.ch)*

†Eawag, Swiss Federal Institute of Aquatic Science and Technology, Department of Aquatic Ecology, 8600 Dübendorf, Switzerland

‡Institute of Integrative Biology, ETH Zürich, 8092 Zürich, Switzerland

§Eawag, Swiss Federal Institute of Aquatic Science and Technology, Department of Surface Waters, 8600 Dübendorf, Switzerland

Associate Editor – Daniel Ariztegui

ABSTRACT

Human activities such as river corrections and deviations, lake-level regulations and installations of hydropower plants affect and often strongly modify natural processes in lacustrine systems. In 1714, the previously bypassing Kander River was deviated into peri-alpine Lake Thun. This pioneering geo-engineering project, the first river correction of such dimensions in Switzerland, doubled the water and sediment input to the lake. In order to evaluate the sedimentary consequences of the Kander River deviation, the lacustrine sediments were investigated using a combined approach of high-resolution (3·5 kHz) reflection seismic data and sediment cores (maximum length 2·5 m). The significance of this study is increased by the possible hazard represented by ammunition dumped into the lake (from 1920 to 1960) and by the recent installation of a gas pipeline on the lake floor in 2007/2008. The first 130 years after the river deviation were dominated by an extremely high sediment input, which led to the frequent occurrence of subaquatic mass movements. Slope failures primarily occur due to rapid sediment accumulation, but were occasionally triggered in combination with earthquake-induced shocks and lake-level fluctuations. After 1840, mass-movement activity and sedimentation rates decreased due to a reduced sediment input as the Kander River adjusted to its new base level and, to a smaller degree, by further engineering of the Kander River bed and gravel withdrawal at the Kander Delta. A further consequence of the Kander River deviation is that the shores around Lake Thun have been more frequently affected by flooding due to the increased water input. In the time span from 1850 to 2006, six historically and/or instrumentally documented flood events could be correlated to flood turbidites in the sediment cores. This study demonstrates the significant usefulness of lacustrine sediments, not only in archiving natural hazards and human impact but also in assessing the consequences of future anthropogenic interventions on lacustrine systems.

[1]Present address: Department of Geology and Paleontology and Institut des Sciences de l'Environnement, University of Geneva, 1205 Geneva, Switzerland.

[2]Present address: Department of Biological and Environmental Science, Centre of Excellence in Evolutionary Research, PO Box 35, FI-40014 University of Jyväskylä, Finland.

Keywords 'Kanderschnitt', flood event, lacustrine turbidite deposit, Lake Thun, river engineering, subaquatic mass movement.

INTRODUCTION

The first river engineering projects realized in Switzerland in the 18th and 19th Centuries aimed to regain marshy terrain for agriculture and to prevent the flooding of nearby towns and villages (Vischer, 2003; Nast, 2006). These engineering activities comprised river diversions, as well as modifications of channel geometry and the bed morphology. Such interventions were innovative and brought new land-use opportunities, but the consequences of such drastic interference with river systems were only partly anticipated. River corrections and deviations induced hydrological, sedimentological and ecological, as well as economical and societal changes. Moreover, these actions often created new problems, such as destabilization of river banks and displacement of flooding zones (Vischer, 2003).

The Lake Thun area was affected by the oldest major river correction in Switzerland. This pioneering project was carried out in 1714 and is known as the 'Kanderschnitt'. In order to prevent severe flooding in further downstream areas, the Kander River was redirected into Lake Thun. This action increased the catchment area of the lake by 50% and, therefore, had important consequences for the sedimentary and hydrological budget of the lake.

Lacustrine sediments provide high-resolution archives to reconstruct past anthropogenically induced modifications of lake systems, as well as environmental and climatic changes (e.g. Gaillard *et al.*, 1991; Anselmetti *et al.*, 2007; Mueller *et al.*, 2010). The frequency and intensity of past natural catastrophes, such as flood events, earthquakes and subaquatic mass movements, can be inferred in detail from the lacustrine sediment record (e.g. Siegenthaler & Sturm, 1991; Noren *et al.*, 2002; Schnellmann *et al.*, 2006; Bertrand *et al.*, 2008). Nowadays, the occurrence and severity of natural disasters may be influenced by human activities that change the boundary conditions of lake systems. Hence, sediment-based event records can also reflect human activity, such as river corrections and deviations, lake-level and river-discharge regulations, as well as gravel withdrawal at river deltas (Arnaud *et al.*, 2003; Anselmetti *et al.*, 2007; Strasser & Anselmetti, 2008). In this context, the sediments of Lake Thun provide an ideal record of natural hazards and human impacts, as well as of their possible interrelations.

Recently, Lake Thun has also attracted attention because of gonadal malformations in lake whitefish (*Coregonus* sp.). One of the several possible causes for such deformations could be contamination by ammunition residues (Bernet *et al.*, 2008; Bogdal *et al.*, 2009), because 4600 t of army ammunitions were dumped into the lake between 1920 and 1963 (Eidgenössisches Departement für Verteidigung, Bevölkerungsschutz und Sport, 2004), also increasing the environmental risk of mass movements. This hazard, as well as a 15 km long gas pipeline installed on the sediment surface in 2007 and 2008 (Erdgas Thunersee AG, 2009), provides an additional reason to study the sediment record and history of the lake. Moreover, the sediments of Lake Thun have not been investigated since the 1970s (Matter *et al.*, 1971; Sturm & Matter, 1972) and analytical and dating methods have improved since then.

The goal of the present study is to document the sedimentation history of Lake Thun since the deviation of the Kander River, based on high-resolution (3·5 kHz) reflection seismic data and sediment core material (maximum 2·5 m core length). The emphasis is placed on documenting the primary sedimentary changes induced by the Kander River deviation, but also on demonstrating the development of the sedimentary system in the subsequent 300 years, particularly regarding the frequency of flood and subaquatic mass-movement events.

STUDY AREA

Geological setting

Lake Thun is situated in the Canton of Bern within the frontal region of the Swiss Alps (Figs 1 and 2; Table 1). The catchment area comprises tectonic units of the Helvetic, Penninic and Molasse domain, along with a minor part of the Aar massif (Bundesamt für Wasser und

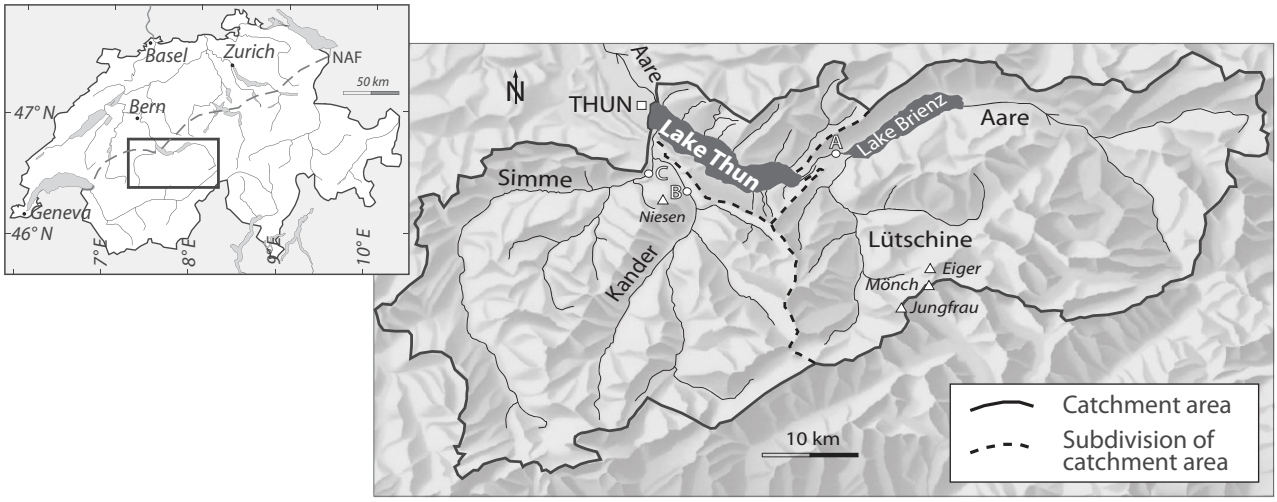

Fig. 1. Location of study area and shaded relief map of Lake Thun catchment area with dashed lines indicating the catchment boundaries of the Aare River, Kander River and remaining smaller Lake Thun tributaries. Capital letters ('A', 'B' and 'C') show the locations of the gauging stations used in Table 1 and Fig. 12B. NAF, North-Alpine nappe front.

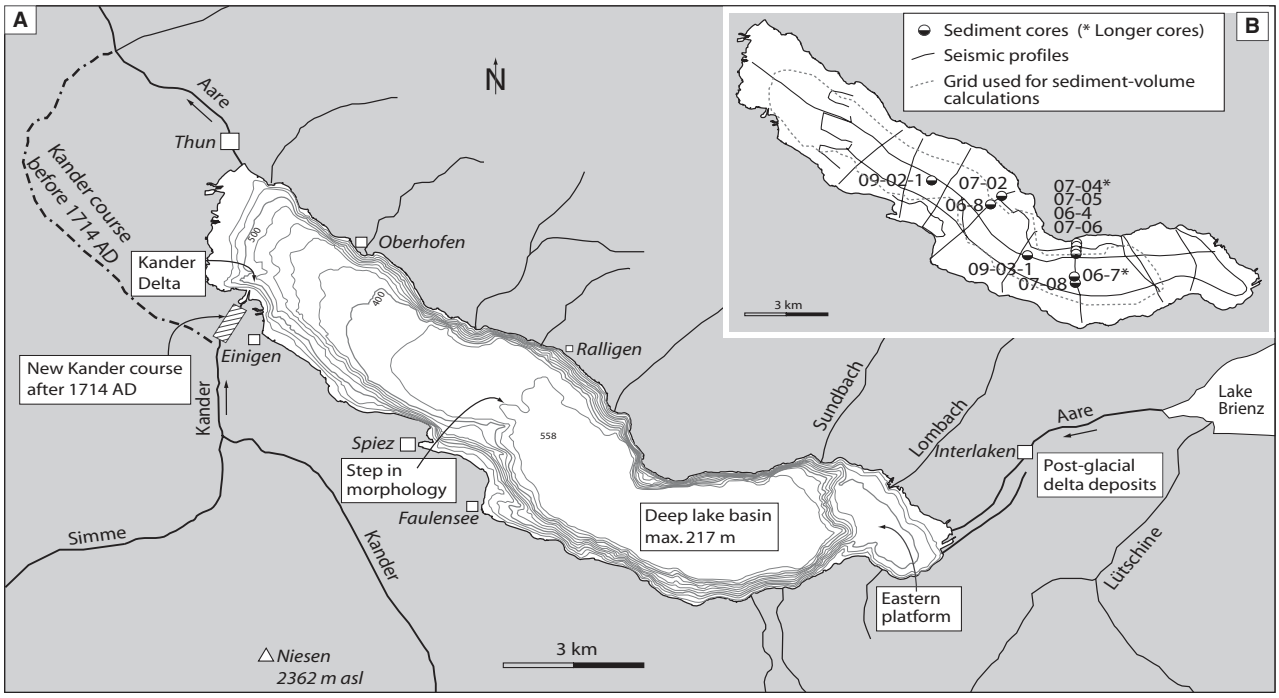

Fig. 2. (A) Bathymetric map of Lake Thun with tributaries, cities and main villages. The Kander course before and after the river deviation in 1714 is indicated. (B) Map of sediment core locations and grid of 3·5 kHz pinger seismic profiles. The dashed line represents the dimensions of the grid used for sediment volume calculations.

Geologie, 2005b). The Kander catchment area is characterized by Penninic (Klippen, Simme and Niesen nappes) and Helvetic (Wildhorn and Diablerets nappes) units. The Klippen, Wildhorn and Diablerets nappes are dominated by siliceous, marly and massive limestones of Mesozoic age, whereas the Simme and Niesen nappes comprise Flysch deposits of Cretaceous to Eocene age (Bundesamt für Wasser und Geologie, 2005a; Froitzheim *et al.*, 2008). The Kander catchment area therefore contains sedimentary lithologies that are responsive to both chemical and mechanical denudation: the limestones represent a major carbonate source to the lake, whereas the

Table 1. Physical characteristics of Lake Thun and its catchment area (Bundesamt für Umwelt, 1903 to 2007; Sturm & Matter, 1972; Amt für Gewässerschutz und Abfallwirtschaft des Kantons Bern, 2003).

Surface area	47·69 km^2	Maximum water depth	217 m
Surface elevation	558 m a.s.l.	Average water depth	136 m
Length	17·5 km	Catchment area	2451 km^2
Maximum width	3·5 km	Average elevation of catchment area	1748 m a.s.l.
Water volume	6·42 km^3	Present trophic state	Oligotroph

Tributary	Catchment area (km^2)	Discharge (average 2007) (m^3 s^{-1})	Sediment supply (%)	Water supply (%)	Carbonate content (%)
Aare (A)	1129	59·5	*ca* 0	*ca* 50	<25
Kander and Simme	1120	42·8	*ca* 85	*ca* 40	>45
Kander (B)	496	21·2	*ca* 65	*ca* 20	–
Simme (C)	564	21·6	*ca* 20	*ca* 20	–
Small tributaries	202	10 to 15	*ca* 15	*ca* 10	<20 to >45

Capital letters (A, B and C) refer to locations of gauging stations in Fig. 1.

sandstones (Flysch) provide a fair amount of magmatic and metamorphic minerals to the clastic input of the lake (Sturm & Matter, 1972; Tiefbauamt des Kantons Bern and Amt für Landwirtschaft und Natur des Kantons Bern, 2004; Bundesamt für Wasser und Geologie, 2005b).

The lake basin is an overdeepened valley eroded by the Aare glacier during former alpine glaciations. Post-glacial delta deposits of the Lütschine and Lombach Rivers divided the former single basin into Lake Thun and Lake Brienz (Matter *et al.*, 1971). The basin of Lake Thun can be subdivided into three parts (Fig. 2A): the north-western part is characterized by (i) a gentle slope (0·5° to 1°) starting at the Kander Delta and ending near Spiez, where a step in the lake morphology leads to (ii) the deep part of the lake. This deep central part of Lake Thun has a near uniform water depth of 215 to 217 m. At the eastern end of the lake, the lake bottom ascends to (iii) a platform of intermediate water depth (48 to 78 m), representing the sublacustrine part of the post-glacial delta deposits dividing the basins of Lake Thun and Lake Brienz. The lateral flanks of Lake Thun are steep, especially along the northern shore.

Two main tributaries, the Kander and Aare Rivers, are responsible for 90% of the water supply to Lake Thun (Table 1). The Aare River, which first flows through deep Lake Brienz, arrives in Lake Thun almost free of suspended particles (Sturm & Matter, 1972). Therefore, today, 85% of the sediment supply to Lake Thun is due to the Kander River (Sturm & Matter, 1972), as demonstrated by the development of a large delta deposit at the Kander mouth in the 300 years since the river was diverted into the lake. Estimated values for the sediment load of the Kander River range from 30 to 1000 kt $year^{-1}$ (Steiner, 1953; Niklaus, 1969; Hinderer, 2001; Schlunegger & Hinderer, 2003; Tiefbauamt des Kantons Bern and Amt für Landwirtschaft und Natur des Kantons Bern, 2004), reflecting both scientific uncertainty in the estimates and variations in the sediment load during the 19th and 20th Centuries. One half of the Kander catchment is drained by the Simme River (Fig. 1) which has, on average, a nearly identical water discharge to the upstream Kander (both *ca* 21 m^3 s^{-1}) but a lower sediment transportation capacity due to a smaller river slope (Schlunegger & Hinderer, 2003). Remnant water input (10%) and sediment load (15%) of the Lake Thun catchment area derive from small tributaries (Figs 1 and 2A) along the northern and southern shores of the lake, of which the Lombach River is the largest.

The Kander River deviation ('Kanderschnitt', 1714)

The deviation of the Kander River into Lake Thun, completed in 1714, was the first major river modification in Switzerland (Vischer, 2003). Prior to 1714, the Kander River flowed into the Aare River 2·5 km downstream of the city of Thun (Fig. 2A; Vischer, 2003). It regularly flooded villages along its way and also dammed the Aare River (outflow of Lake Thun) at the confluence by delivering large sediment loads. To solve these flooding problems, the decision was taken to lead the Kander River directly into Lake Thun by digging a channel through the moraine hill near

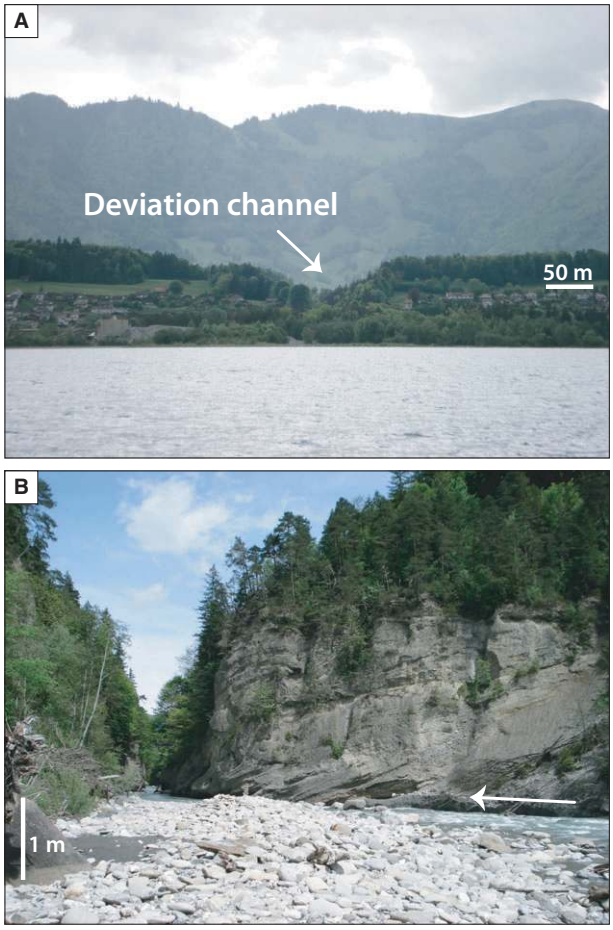

Fig. 3. Photographs illustrating the incision channel through the moraine hill produced by the Kander River deviation. (A) Depression in the moraine ridge due to the deviation channel seen from the lake. (B) Entry into the deviation channel, walls are up to 45 m high. The white arrow indicates water flow direction.

the town of Einigen (Figs 2A and 3). The river deviation corresponded to a shortening of the Kander course by 8 km, thus steepening the river gradient downstream of the deviation site and increasing the stream power and the bed shear. This effect led to strong erosion and high incision rates in the channel, as well as to a higher sediment transport capacity. In 1716, the river bed in the new channel was already at a level 27 m below its projected depth and, at present, it is situated 40 m lower than projected (Tiefbauamt des Kantons Bern and Amt für Landwirtschaft und Natur des Kantons Bern, 2004). Incision rates increased not only in the diversion channel itself but also progressively in upstream reaches of the Kander River. Observations indicate that the river bed of today is situated 20 to 30 m below the level in 1714, at least in the lowest 10 km of the course of the Kander (Tiefbauamt des Kantons Bern and Amt für Landwirtschaft und Natur des Kantons Bern, 2004). As a further consequence, the doubling of the water flow into Lake Thun increased the frequency of severe floods in the city of Thun located at the outflow of the lake. New water gates to control these Kander floods were completed in 1726 and improved in 1788 (Vischer, 2003). In the 19th and 20th Centuries, numerous engineering interventions on the Kander River bed were performed, aiming to decrease the energy level of the river and, thus, to reduce the threat and damage due to floods.

METHODS

High-resolution reflection seismic data

A reflection seismic grid consisting of *ca* 70 km of seismic profiles (Fig. 2B) was acquired in May 2007 using a 3·5 kHz pinger source fixed on an inflatable catamaran that was pushed in front of a small vessel. The seismic profiles were recorded digitally in SEG-Y format using a global positioning system (GPS; error ± 5 m) for navigation. Seismic data were processed with SPW™ (Seismic Processing Workshop; Parallel Geoscience Corp., California City, CA, USA) software including band-pass filtering (2·2 to 6·3 kHz). The time-depth conversion in water and sediment is based on a p-wave velocity of 1450 m s^{-1}, resulting in a theoretical vertical resolution of 10 to 20 cm at the applied frequency (Rayleigh, 1885). Interpretation of seismic data was accomplished with KingdomSuite™ 8.1 (Sesimic Micro-Technology, Houston, TX, USA). Defined seismic horizons were imported into SURFER™ software (RockWare, Golden, CO, USA) to create grids for sediment thickness and volume calculations.

Sediment core analysis

Sediment cores (Fig. 2B) were collected in October 2006, May 2007 and June 2009 using a gravity corer (maximum core length 130 cm) and a modified gravity corer that is equipped with an additional weight for hammering (maximum reached core length 255 cm). However, hammering on top of the instrument, gas expansion and the use of a core catcher induced compression and disturbances in the longer core material.

Bulk density, magnetic susceptibility and p-wave velocity of the sediment material were measured at 0·5 cm resolution on unsplit cores

using a multi-sensor core logger (MSCL) (Geotek Limited, Daventry, UK). After cores were split, the fresh sediment surface was photographed, macroscopically described and sampled. Particle-size analysis of bulk sediment was carried out using a Mastersizer 2000 (Malvern Instruments Limited, Malvern, UK) laser diffraction instrument measuring particle sizes from 0·02 to 2000 μm. Total carbon (TC) and total inorganic carbon (TIC) content was analysed using a 5012 Coulometer (UIC Inc., Joliet, IL, USA) measuring the CO_2 content derived from previously freeze-dried samples by burning (TC) and acidification (TIC). Total organic carbon (TOC) was then calculated as the difference between TC and TIC. X-ray fluorescence (XRF) core scanning (instrument from Avaatech, Den Burg, The Netherlands) at 1 cm resolution provided a rapid non-destructive means of analysing the elemental composition of sediment material. X-ray fluorescence core-scanning results are semi-quantitative and are presented as *intensity* (Richter *et al.*, 2006; Weltje & Tjallingii, 2008).

SEISMIC STRATIGRAPHY

Seismic penetration reaches 60 m in the deep lake basin, imaging a well-stratified thick sediment succession (Fig. 4A). Towards the Kander Delta, seismic penetration generally decreases and the acoustic facies becomes more chaotic/transparent (Fig. 4B to D). Minimal or no seismic penetration is observed on the steep lake flanks and at the north-western and eastern ends of the lake, where proximal delta sediments are deposited (Kander Delta, Eastern platform; Fig. 2A).

The seismic record is divided into four seismic Sequences (from top to bottom S1 to S4) that are delimited by seismic Horizons a, b and c (Figs 4 and 5; letters in white squares). The lower limit of Sequence S4 is not defined, as seismic imaging did not reach the base (i.e. bedrock/moraine) of the lacustrine sediment cover. Seismic Horizons d, e and f represent the top reflections of three major disturbed seismic units within Sequence S4 (Fig. 5).

Sequence S1

Sequence S1 comprises the top package of the sediment cover mostly characterized by parallel, continuous and high-amplitude reflections (Fig. 4A to C). However, the base of Sequence S1 consists of a partly low-amplitude to transparent facies, which is more prominent in the north-western part of the lake than in the deep lake basin. In addition, seismic reflections in the north-western lake part have an undulating/hummocky shape (Fig. 4B to D). The sediment thickness map of Sequence S1 confirms a relatively uniform sediment distribution with a slight increase in thickness towards the north-west (Fig. 6A).

Sequence S2

Sequence S2 is characterized by contrasting seismic facies between the deep lake basin and the north-western part of the lake. In the deep lake basin, its lower and upper boundaries are, respectively, defined by the base-reflection and top-reflection of a well-stratified sediment package onlapping towards the northern shore (Fig. 4A). Within this onlapping package, high-amplitude reflections alternate with thin transparent intervals. In the north-western part of the lake, Sequence S2 presents a chaotic/transparent facies that covers most of the sub-surface slope (bounded by a white line; Fig. 4B to D). This

Fig. 4. Interpreted 3·5 kHz reflection seismic profiles of Lake Thun focussing on the onset of the Kander River input. The small map of the lake shows the location of profiles presented in this figure (grey) and Fig. 5 (black). S1 to S4 are defined seismic Sequences, 'a' to 'f' represent seismic Horizons. Dashed lines indicate bases of chaotic/transparent units. (A) Crossing seismic profile demonstrating the excellent seismic penetration in the deep lake basin. Note the uniform sediment distribution of Sequence S1. Sequence S2 shows an internal onlap geometry with interlayering of high-amplitude reflections and thin transparent intervals. In Sequence S3, sediment accumulation is highest at the northern shore, contrasting to Sequence S2. Sequence S4 shows a comparatively even thickness distribution across the lake basin. Also note the absence of large mass-movement deposits in all seismic sequences. (B) Longitudinal seismic profile located at the change in slope gradient near Spiez, illustrating the transition from chaotic/transparent deposits (in white) to high-amplitude reflections and intercalated transparent seismic intervals towards the south-east. (C) Transverse seismic profile through the slope in front of the Kander Delta, with large chaotic/transparent deposits marked in white (in S2) and below Horizon 'c'. (D) Longitudinal profile along the slope in the north-western part of the lake, presenting chaotic/transparent deposits (in white) building up most of Sequence S2 and contrasting to the overlying undulating reflections of Sequence S1. Note also the thinning of Sequence S2 towards the morphobathymetric step near Spiez.

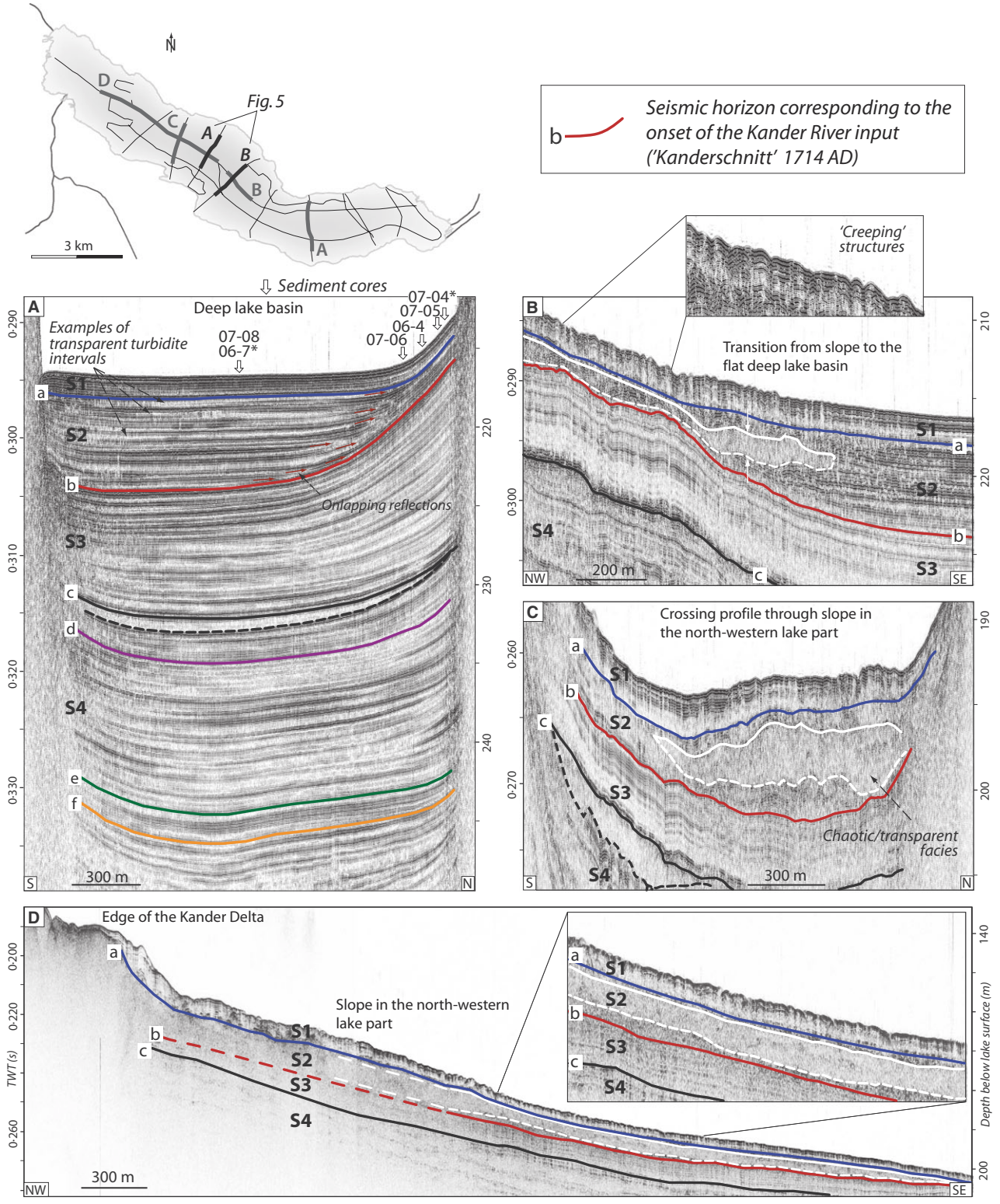

seismic facies is typical for mass-movement deposits (Nakajiama & Kanai, 2000; Schnellmann *et al.*, 2002). The thickness map of Sequence S2 documents strong lateral differences in sedimentation (Fig. 6B): the sediment is up to 7 m thick in the central and southern part of the deep lake basin, then decreases at the morphological step near Spiez (2 to 5 m) and steadily regains thickness on the slope towards the Kander Delta (12 to 14 m).

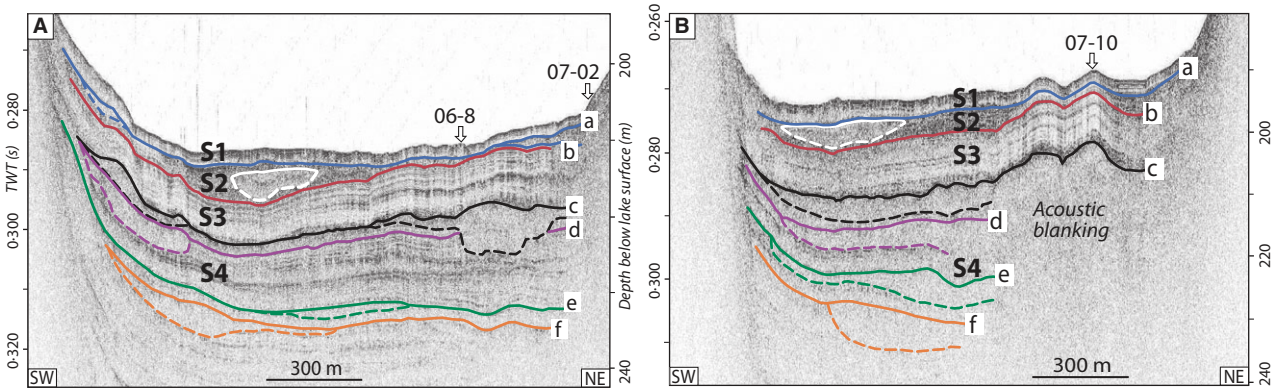

Fig. 5. Interpreted 3·5 kHz reflection seismic profiles of Lake Thun presenting the full range of seismic penetration. For details and location of profiles, see Fig. 4. (A) Crossing profile locating chaotic/transparent bodies that define event Horizons 'c' to 'f' and chaotic/transparent body inside S2 (marked in white). (B) Crossing seismic profile specifically highlighting a transparent seismic section (acoustic blanking) in the northern third covered by Horizon 'c'.

Sequence S3

Sequence S3 shows parallel seismic reflections of varying amplitudes. Reflections are more clearly shaped in the deep lake basin than in the north-western part of the lake which is due, at least partly, to the overlying chaotic deposits of Sequence S2 attenuating the seismic waves. In the north-west, the base of Sequence S3 (i.e. Horizon c) is defined by the top of large mass-movement deposits with a chaotic/transparent facies (Figs 4C and 5). At the same seismostratigraphic level, a complete acoustic blanking of the deeper units in the northern third of the crossing seismic profile near Spiez occurs, yielding no stratigraphic information (Fig. 5B). The acoustic blanking is probably due to gas-rich sediment or to rock debris (for example, rock fall material) preventing deeper penetration of acoustic energy. In the deep lake basin, seismic Horizon c covers a transparent interval thinning out towards the north (Fig. 4A). In contrast to Sequences S1 and S2, the thickness map of Sequence S3 (Fig. 6C) presents a maximum sediment thickness in the eastern and northern part of the deep lake basin (10 to 14 m). From there, the thickness constantly decreases towards the north-west (<6 m).

Sequence S4

The sediment package below seismic Horizon c consists of Sequence S4. In the deep lake basin, seismic reflections are continuous and regularly layered (Fig. 4A). In contrast, three prominent seismic subunits with chaotic/transparent facies interrupt the layering of the reflections in the north-western part of the lake (Fig. 5); they are

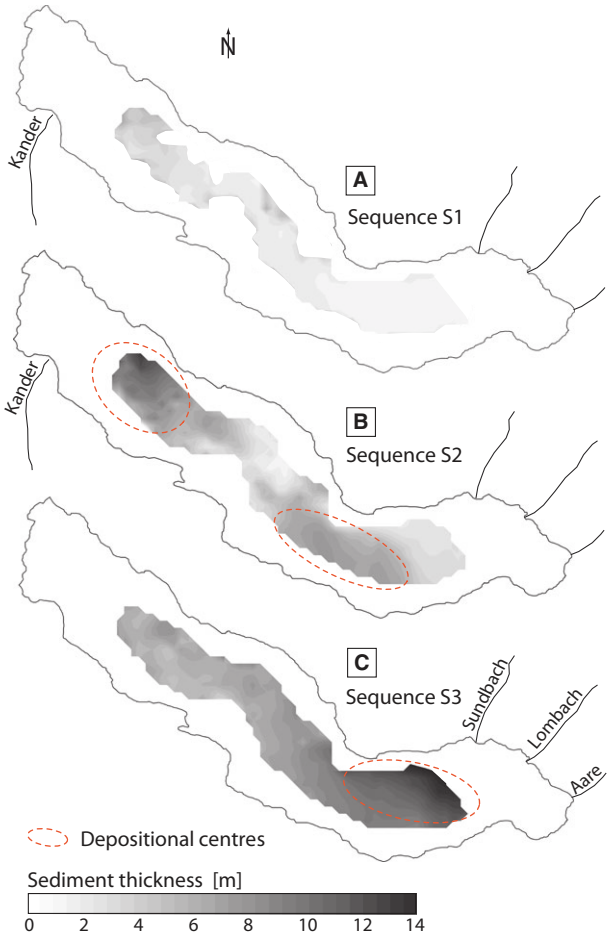

Fig. 6. Sediment thickness maps of seismic Sequences (A) S1, (B) S2 and (C) S3, illustrating sediment distribution changes within the lake basin. Labelled rivers provide the main sediment input during the correspondent sequence. Maps were calculated from seismic data with a velocity of 1450 m s^{-1}. Data are only available where seismic Horizons 'a', 'b' and 'c' are defined.

typical for mass-movement deposits. The high-amplitude reflections bounding the top of the chaotic/transparent units are defined as seismic Horizons d, e and f, representing the seismo-stratigraphic level of the events. Horizons d, e and f can be followed to the deep lake basin, where they overlie, similar to Sequence S2, thin transparent intervals expanding over the entire width of the lake basin (Fig. 4A).

SEDIMENT CORE RECORD

A selection of 10 sediment cores were used for this study, eight gravity short cores and two longer cores retrieved with the manual percussion system (Fig. 2B). The sediment material is composed mainly of authigenic calcite and detrital deposits but is poor in organic material, except in the most recent interval.

Lithotypes

Four lithotypes (I to IV) were differentiated to characterize the sediment succession (Fig. 7).

Regular background sediments (Lithotype I)
The regular background sediments consist of fine-grained (grain size 4 to 7 μm) light-grey authigenic calcite interlayered with millimetre to sub-millimetre thick brownish, yellowish or dark greyish laminae of detrital origin.

Graded deposits (Lithotypes II and III)
Graded deposits also show variable colours and consist of detrital material, but are thicker than the laminae of the background sediments and contain normally or inversely graded sections. Grain sizes range from coarse sand to clay.

Thin graded deposits (Lithotype II) are 2 to 5 mm thick and show only faint grading. These deposits probably derive from floods of small tributaries leading to local distribution of the sediment load or representing the distal deposition of flood material from larger tributaries. Thick graded deposits (Lithotype III), >5 mm thick, are clearly graded with coarse sand to silt-sized basal and finer silt to clay-sized upper parts; they are often topped by a thin clay cap and are interpreted as turbidity current-generated (underflows) deposits. In such lake environments, turbidity currents are due to large flood events or subaquatic mass movements (Siegenthaler & Sturm, 1991; Mulder & Alexander, 2001; Beck, 2009). Accordingly, graded deposits are based on grain-size analysis, characterized as flood-related (Lithotype IIIA) or mass-movement-related turbidites (Lithotype IIIB).

Organic-rich sediments (Lithotype IV)
Organic-rich deposits characterized by the black colour of the fresh, unoxidized sediment surface reflect anthropogenically induced lake eutrophication, during which enhanced nutrient supply led to an increase in biological productivity (for details on this lithotype, see Wirth, 2008; Rellstab *et al.*, 2011). This interval is situated at core depths between 10 and 50 cm.

Turbidite deposits

A precondition for the reconstruction of the event history of Lake Thun is the ability to distinguish between flood-related and mass-movement-related turbidite deposits (Lithotypes IIIA and IIIB). This classification of the turbidites is based on grain-size distributions, the thickness evolution within the core transect and observations in the seismic data. Furthermore, the results are compared to former studies discussing the different types of turbidites in lacustrine and fjord environments (Siegenthaler & Sturm, 1991; Gorsline *et al.*, 2000; St-Onge *et al.*, 2004; Beck, 2009).

Grain-size distributions
Flood-related turbidite deposits consist of normally and potentially inversely graded sections (Mulder & Alexander, 2001; Mulder *et al.*, 2003; St-Onge *et al.*, 2004; Gilli *et al.*, 2011, in press). Coarsening-up sections result from high-magnitude flood events (Mulder *et al.*, 2003), reflecting increasing and peak water discharges. The concluding section at the top of a flood turbidite consists of a fining-up section mostly completed by a light-coloured clay cap representing the final fine-grained fallout (Gilli *et al.*, 2003; Mulder *et al.*, 2003; Girardclos *et al.*, 2007). Furthermore, grain-size changes occur gradually, reflecting the dynamic increase and decline of the river discharge (Mulder *et al.*, 2003; Beck, 2009).

In contrast, subaquatic mass movements primarily produce chaotic mass flows from which a suspension cloud evolves, providing the material for turbidites or even megaturbidites (Siegenthaler *et al.*, 1987; St-Onge *et al.*, 2004; Schnellmann *et al.*, 2006). The focused release of the sediment in one specific moment leads to high sediment concentrations in the suspension cloud and, therefore, enables a separation of fine-grained and coarse-grained material (Shiki *et al.*,

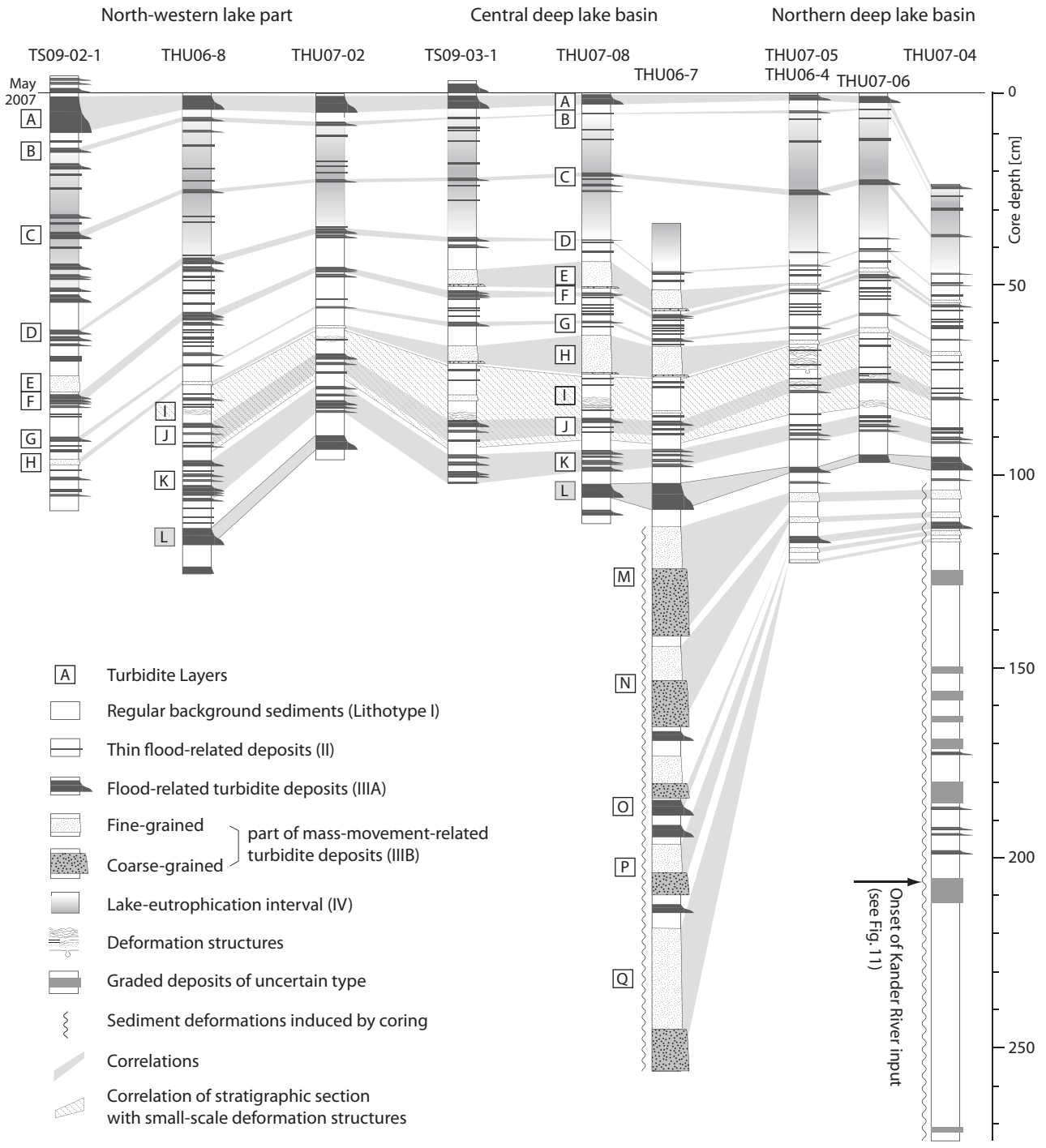

Fig. 7. Core to core correlation with Lithotypes I to IV presented as a transect through the lake basin. For Lithotypes II and III, only deposits thicker than 5 mm are included. Longer cores, lacking the sediment top and being compressed due to hammering, are aligned to Layer L in corresponding gravity short cores.

2000; Mulder *et al.*, 2003). This observation results in initial settlement of the coarse fraction and a secondary settlement of the finer suspended material in the deepest part of the lake basin (Siegenthaler *et al.*, 1987). Hence, the transition from the coarse-grained basal part to the finer-grained upper part is characterized by a sharp decrease in grain size (Siegenthaler & Sturm, 1991; Chapron *et al.*, 1999; Bertrand *et al.*, 2008; Beck, 2009). The coarser basal part may show fluctuations in grain size generated by a seiche wave (Siegenthaler *et al.*, 1987; Schnellmann

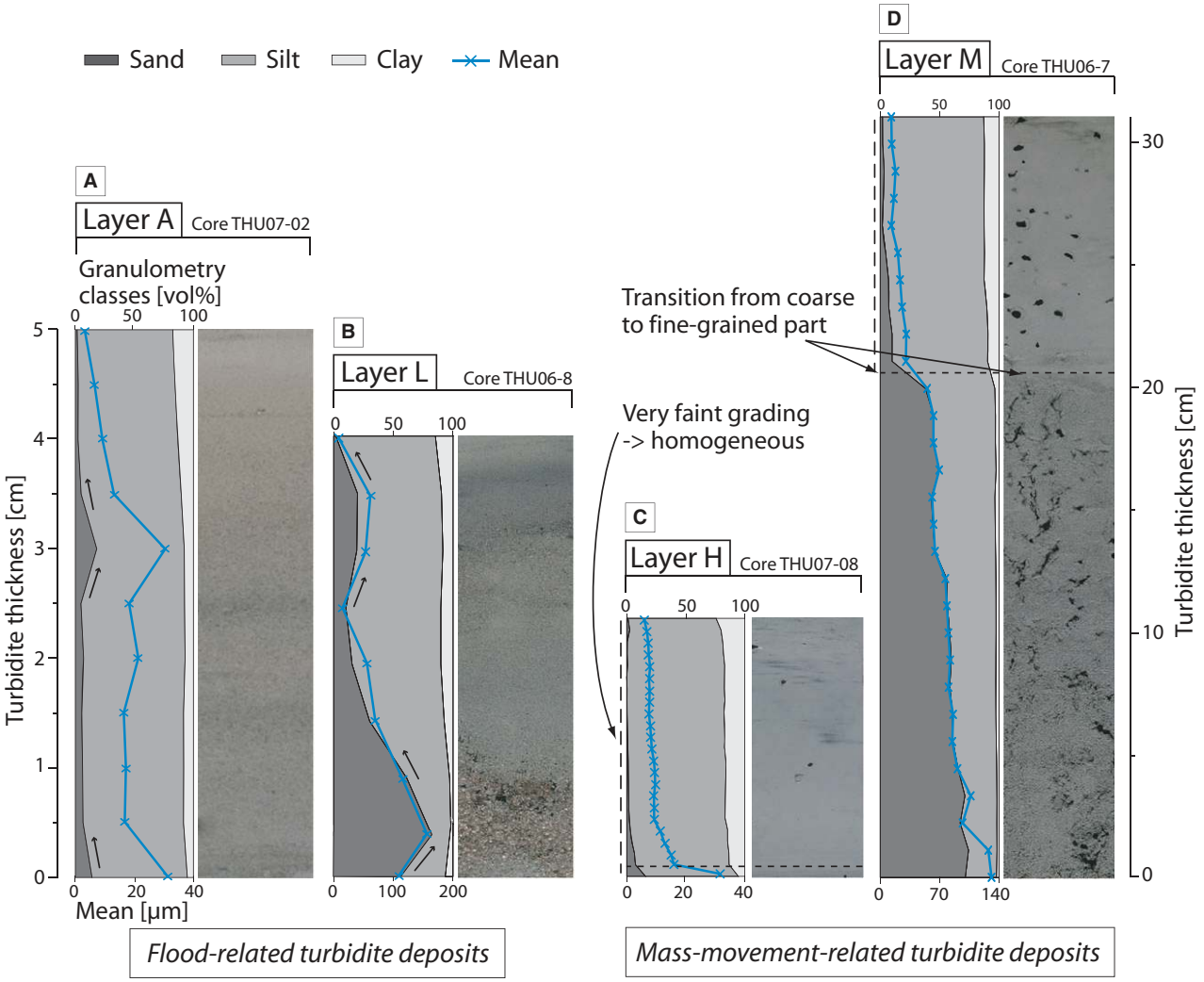

Fig. 8. Grain-size distributions of flood-movement and mass-movement-related turbidite deposits. Turbidite layers ('A', 'H', 'L' and 'M') correspond to labelling in core to core correlation (Fig. 7; for core locations refer to Fig. 2B). Sampling resolution is 0·5 cm for Layers A, H and L, and 1 cm for Layer M. Granulometry classes: clay <2 µm, silt 2 to 63 µm, sand >63 µm. (A) Layer A: flood-related turbidite deposit with pulses of coarser material at the base and at 3 cm thickness. (B) Layer L: flood-related turbidite deposit with inverse grading at the base as a result of the waxing of the river runoff and a second pulse of coarser material at 3 cm. (C) Layer H and (D) Layer M: fine-grained and coarse-grained mass-movement-related turbidite deposit, respectively, both characterized by their large thickness and the clear transition from the coarse-grained to the fine-grained part.

et al., 2006). However, this texture was not observed in Lake Thun. In the upper fine-grained part of the turbidites, the grading is faint to nearly absent. Therefore, these deposits are often also referred to as 'homogenites' (originally introduced by Kastens & Cita, 1981; adopted by, for example, Siegenthaler *et al.*, 1987; Chapron *et al.*, 1999; Bertrand *et al.*, 2008). Based on the sediment volume involved, mass-movement-related turbidites can be significantly thicker than flood-related turbidites (Gorsline *et al.*, 2000).

Examples of turbidite grain-size distributions are presented in Fig. 8. Labelling of deposits is based on turbidite layers used for core to core correlations (Fig. 7). Layers A and L show similar grain-size patterns (Fig. 8A and B). These layers both have the coarsest fraction in the basal part, followed by a fining-up section and a second 'pulse' of coarser material, which is succeeded by the final fining-up section. The main differences are: (i) the overall grain size, as Layer L consists of generally coarser material than Layer A; and (ii) the thin inversely graded section at the base of Layer L. Layer H (Fig. 8C) comprises a thin basal part, overlain by a finer, very homogeneous main body and a clay cap on top. Layer M (Fig. 8D)

shows a very coarse (sand to coarse silt) and thick basal part contrasting with a finer-grained upper part (mainly silt with some clay). This contrast between the basal and upper parts, which have different surface textures, is easily distinguished on the core photograph. The grain-size pattern of Layer M resembles that of Layer H; however, the coarser part is considerably thicker and grain size generally is coarser.

Based on these observations, Layers A and L are interpreted as flood-related turbidites; they contain inversely graded sections and gradually occurring grain-size changes (as presented in Mulder *et al.*, 2003; St-Onge *et al.*, 2004; Beck, 2009). Layers H and M are typical for mass-movement-related turbidites because of the larger thickness and the clear transition from the coarser basal part to the finer and fairly homogeneous upper part. Layer H strongly resembles the 'homogenite' described by Chapron *et al.* (1999) in Lake Le Bourget, and Layer M corresponds to megaturbidites observed in Lake Lucerne (Siegenthaler & Sturm, 1991; Schnellmann *et al.*, 2006). In an analogous manner, all relevant turbidite deposits in the sediment core record could be classified as either flood-induced or mass-movement-induced.

Core to core correlation and turbidite deposition

The core to core correlation (Fig. 7) is based on the stratigraphy of graded deposits (Lithotypes II and III) and is achieved by visual observation of their sedimentary characteristics, such as bed thickness, grain-size distribution, grading and colour. Stratigraphic layers are arranged in single turbidites or bundles of turbidites and are labelled with capital letters (Layers A to Q).

The core transect illustrates that prominent flood turbidites are thickest in the north-western part of the lake and decrease in thickness towards the deep lake basin, indicating that the sediment source is located at the north-western end of the lake (Fig. 7). In contrast, mass-movement turbidites are thickest in the centre of the deep basin. Here, seismic data are used to reconstruct the sediment distribution mechanism. These data show a chaotic/transparent facies typical for mass-flow deposits in seismic Sequence S2 on the slope in the north-western part of the lake (Fig. 4D). This chaotic/transparent facies passes into high-amplitude reflections intercalated with transparent sections at the morpho-bathymetric step to the deep basin, representing the turbidites that settled out from the suspension cloud (Fig. 4A and B). Thus, the source area of the mass-movement material is, similar to the flood material, the north-western end of the lake. These observations correspond to the deposition model for mass-wasting material presented by Siegenthaler *et al.* (1987) and adopted by, for example, Schnellmann *et al.* (2006) and Bertrand *et al.* (2008), demonstrating that the chaotic deposits of the mass flow become overlain by massive turbidite deposits. However, Lake Thun differs from these studies in the spatial separation of mass-flow and turbidite deposits. This separation is probably due to the morphology of the lake basin and the large distance between the source area and the deepest part of the lake.

Small-scale deformation structures

Most of the short cores include a *ca* 15 cm thick stratigraphic interval (Layer I; Figs 7 and 9) showing disturbed layering, microfaults and liquefaction structures. The most remarkable deformation structures are (Fig. 9): (i) a sediment section full of microfaults and disrupted material; (ii) a mushroom-like intrusion in core THU07-05; (iii) a structure in core THU07-06, illustrating the liquefaction of a sandy turbidite, provoking the rupture and sinking down of the layer situated above; and (iv) microfaults in core THU07-02. Longer cores were not considered for these detailed observations, because coring artefacts due to hammering, gas expansion and core catcher induced strong deformations overprinting the original sediment structures.

Previous work in Swiss lakes and other study areas report similar deformation structures in relation to earthquake events (Youd, 1973; Monecke *et al.*, 2004). The occurrence of the deformation structures throughout the cores at the same stratigraphic level determines earthquake-induced lake bottom shaking as a likely trigger mechanism. This interpretation is strengthened by a mass-movement-related turbidite (Layer H; Fig. 7) sitting on top of the deformed stratigraphic interval.

^{137}Cs dating

In order to date core THU06-4, ^{137}Cs activity was measured at 1 cm resolution from 0 to 41 cm and at 2 cm resolution from 41 to 53 cm core depth (Fig. 10). Results reveal two clear activity peaks corresponding to 1963, the maximum fallout of ^{137}Cs due to atmospheric nuclear weapons testing, and to 1986, the Chernobyl nuclear power

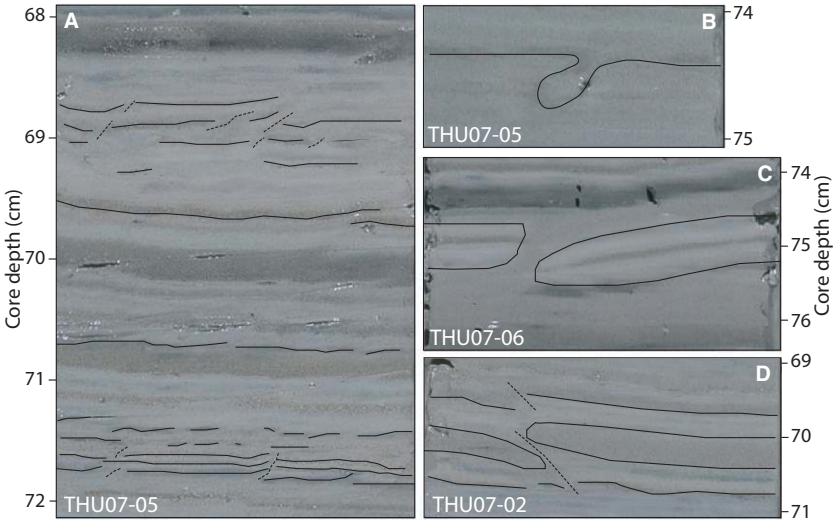

Fig. 9. Small-scale deformation structures provoked by earthquake-induced lake bottom shaking (Obermeier, 1996; Monecke *et al.*, 2004). For description of the structures see text, for position in the core transect, refer to Fig. 7 (Layer I). Core labels and depth in core indicated in white and black lettering, respectively.

plant accident, at 29·5 cm and 13·5 cm core depth, respectively. The zero ^{137}Cs activity at 38 cm is associated with the start of the atmospheric nuclear weapon testing in the years 1951 to 1954 (Appleby, 2001). Average sedimentation rate is *ca* 0·7 cm year^{-1} between 1951 and 2006 in core THU06-4. The correlation of ^{137}Cs dates to other cores results in a range of sedimentation rates from 0·6 cm year^{-1} (THU07-02) to 0·9 cm year^{-1} (TS09-02-01) for the same time period.

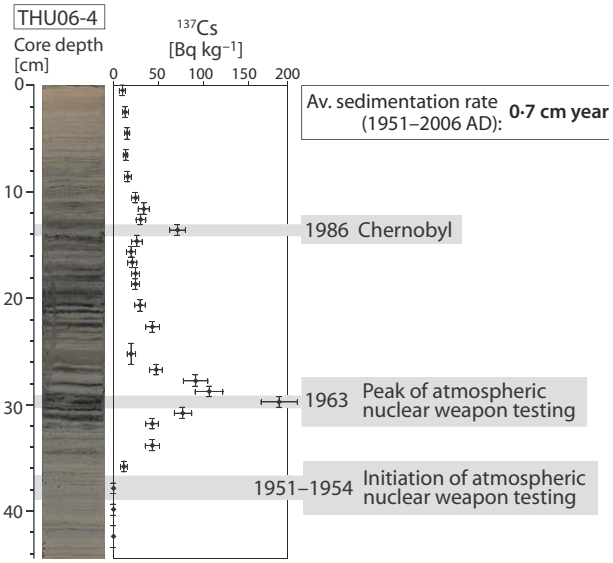

Fig. 10. ^{137}Cs activity curve and sediment core picture of THU06-4 with 1986 Chernobyl and 1963 atmospheric nuclear test peaks. First zero values define the period of onset of atmospheric nuclear testing (1951 to 1954).

SEDIMENTOLOGICAL EVIDENCE FOR THE KANDER RIVER DEVIATION

A combined approach of seismic data and sediment core analysis is used to assess the primary impact of the Kander River deviation on the sedimentary system of the lake.

Evidence in seismic data

Seismic sequence stratigraphy highlights a major change in lake sedimentation at the transition from Sequence S3 to S2 in the form of the following three features: (i) the onlapping S2 reflection terminations onto the S3/S2 boundary in the deep basin (Figs 4A and 11A); (ii) the shift of the depositional centre (Fig. 6B and C); and (iii) the presence of a massive chaotic/transparent body representing the main part of Sequence S2 in the north-western part of the lake (Fig. 4C and D).

The onlap geometry and the shift of the depositional centre indicate a change in the main sediment input. During Sequence S3, the rivers at the eastern end of the lake, the Lombach, Aare and Sundbach Rivers, are certainly responsible for most of the sediment input (Figs 2A and 6C). During Sequence S2, the sediment supply from rivers at the eastern end of the lake is proportionally reduced due to a new sediment input coming from another direction. The depositional centre of Sequence S2 in the north-western part of the lake points to a new sediment source from the north-west, which is interpreted as the Kander River (Fig. 6B).

The additional depositional centre in the central and southern part of the deep lake basin is

explained by increased sediment accumulation due to mass-movement-related turbidites. These turbidites are seismically imaged by the transparent intervals interbedding with high-amplitude reflections (Fig. 4A; Kastens & Cita, 1981; Siegenthaler *et al.*, 1987; Chapron *et al.*, 1999; Hieke, 2000; Schnellmann *et al.*, 2002). The large number of such seismically transparent intervals in the deep lake basin points towards frequent mass-movement events during Sequence S2 (Fig. 4A). Seismic profiles demonstrate that the mobilization of sediment material occurred in the north-western part of the lake, illustrated by the large seismic unit with chaotic/transparent facies in that part of the lake (Fig. 4D). Accordingly, the mass-movement-related turbidites in the deep lake basin represent the distal deposits of the mobilized sediment material. However, in contrast to the numerous turbidite horizons, the north-western part of the lake displays only one 'merged' chaotic/transparent seismic unit with almost no internal divisions (Fig. 4B to D), suggesting that the observed mass-movement body was reworked by numerous mass-movement events.

The change in direction of the sediment input and the shift of the depositional centre, as well as the intensification of the mass-movement activity, are interpreted as being induced by the sudden onset of the intense sediment input of the diverted Kander River. This effect defines seismic Horizon b as the seismostratigraphic level corresponding to the Kander River deviation.

Lithological evidence from the core record

Seismic to core correlations on the crossing seismic profile in the deep lake basin (Fig. 4A) define the position of sequence boundaries S1/S2 (Horizon a) and S2/S3 (Horizon b) in the sediment cores THU06-7 and THU07-04 (Fig. 11A). At the location of core THU06-7, the S1/S2 boundary is correlated to Layer L (Fig. 11A), and the underlying seismically transparent intervals correspond to mass-movement-related turbidite deposits (Layers H, M, N, P and Q). This observation confirms the present seismic facies interpretation (see above).

At the lateral location of core THU07-04, this sequence of mass-movement-related turbidites is condensed, thus proportionally reducing the sedimentation rate (Figs 6B, 7 and 11A). The slope position of core THU07-04 does not allow a very precise seismic to core correlation, but the core record reaches the S2/S3 boundary at *ca* 2 m depth. As THU07-04 did not display any obvious sedimentological changes revealing the new Kander River input, the lower part of core THU07-04 (172 to 232 cm core depth) was investigated for changes in magnetic susceptibility, elemental distribution (XRF core scanning) and concentrations of TIC and TOC (Fig. 11B).

From 232 to 208 cm core depth, magnetic susceptibility fluctuates between 8 and 9·5 SI $\times$ 10^{-5} units. It evolves upcore into slightly lower but very steady values (7·8 to 8·2 SI $\times$ 10^{-5}) from 207 cm towards the top of the core. Changes in elemental composition are illustrated by intensities of Ca and the sum of Al, Fe, K and Ti. The latter group is used as a proxy for detrital input (Rothwell *et al.*, 2006; Moreno *et al.*, 2008). The results exhibit a general increase in Ca above 207 cm. Short-interval decreases in Ca intensity above 207 cm are due to turbidite deposits, which enforce the signal of the detrital elements. Carbon analysis shows a strong upcore rise in the TIC concentration at 207 cm core depth, whereas the TOC progression only shows some slight fluctuations between 210 and 200 cm core depth followed above by a low-gradient change to former values.

These results imply a change in Lake Thun sediment properties at 207 cm core depth. The dominance of Ca and the increase in TIC, a measure for carbonate content, as well as the slightly decreasing magnetic susceptibility values indicate that the lake experiences a new major input of calcium carbonate. This input seems to affect primarily the background sediments, that is, the authigenic calcite precipitation, whereas turbidite deposits rather reduce the carbonate signal.

The increased amount of authigenic carbonate is interpreted as being related to the Kander waters entering the lake. The Kander River has a much higher dissolved calcium-carbonate content than the larger rivers entering from the east, that is, the Aare and Lombach Rivers (Table 1). Furthermore, the distribution of high and low carbonate contents in the background sediments and the flood turbidites, respectively, can be explained by the different slope gradients of the Kander and Simme Rivers (see Fig. 1 for locations), as well as by the catchment geology composed of sandy Flysch deposits and various limestones. Erosion and transportation of the sandy lithologies occur mostly in the part of the catchment area drained by the Kander River upstream of the confluence with the Simme River, because the steeper river slope favours

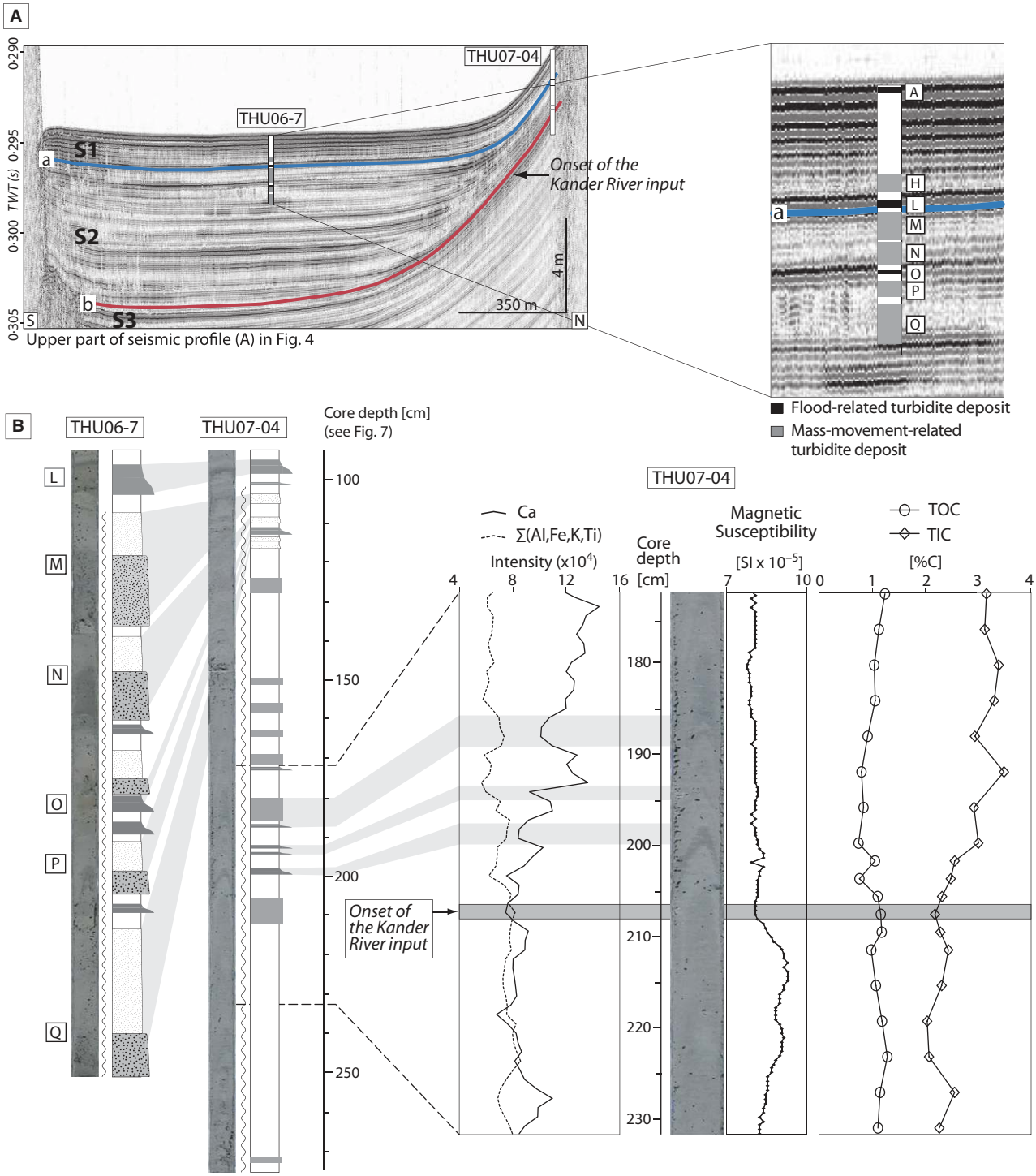

Fig. 11. Onset of the Kander River input in the seismic and sediment core record. (A) Seismic to core correlation for the crossing profile in the deep lake basin showing, with zoom on THU06-7, that Horizon 'a' corresponds to Layer L. Layers A, L and O, interpreted as flood-related turbidites, correspond to reflections with strong positive amplitudes, whereas H, M, N, P and Q, interpreted as mass-movement-related turbidites, correlate to transparent seismic intervals. (B) Photographs and lithology of correlated cores THU06-7 and THU07-04 below 100 cm core depth (lithology legend in Fig. 7). XRF core-scanning data, magnetic susceptibility measurements and carbon analysis (TIC and TOC) on a section of core THU07-04 define the onset of the Kander River input at a depth of 207 cm.

mechanical denudation, as well as the transportation of bed and suspension load. In the Simme catchment, chemical dissolution of limestones and the transport of dissolved river load are predominant. According to Schlunegger & Hinderer (2003), the mechanical denudation in the Upper Kander catchment area accounts for 82% of the total denudation, whereas, in the Simme catchment, only 26% of the denudation is due to mechanical weathering. Thus, the input of Ca and carbonate ions to the Kander River occurs in a continuous mode and probably derives mainly from the Simme catchment. This is in contrast to the concentrated input of the detrital siliciclastic fraction (from sandstones) that may be mobilized primarily in the Kander catchment. The transport of this siliciclastic bed and suspended load requires a more intense river runoff and, therefore, is focused in the case of flood events.

The core depth of the calcium-carbonate increase coincides with the depth of seismic Horizon b, within an error range associated with the compression of core material and a possible offset between the seismic line and coring location due to the large water depth (Fig. 11A). In conclusion, results from sediment core analysis paired with the seismic to core correlation confirm that the above proposed seismostratigraphic level of Horizon b corresponds to the occurrence of the Kander River deviation.

RECONSTRUCTED EVENT HISTORY SINCE THE KANDER RIVER DEVIATION

Since 1714, the high water and sediment input of the Kander River has dominated the sedimentation in Lake Thun and therefore has favoured the enhanced occurrence of strong flood events and subaquatic mass movements. Both processes have distributed sediment material over wide areas of the lake basin.

Major flood events since 1850

The flood history was investigated on the short cores covering the time period 1850 to 2007. Taking into account the sedimentation rates emerging from the time horizons provided by the ^{137}Cs data (Fig. 10), the most prominent flood-related turbidite deposits could be correlated to historic flood events in the Lake Thun area reported by Röthlisberger (1991), as well as to the annual maximal discharge data of the Kander River (Bundesamt für Umwelt, 1903 to 2007). Details about the flood events in 2005 and 1999 that are not covered in Röthlisberger (1991) are provided by federal reports (Bundesamt für Wasser und Geologie, 1999, 2005c). Floods of the Kander River are considered for this correlation, because the decrease in thickness of the flood turbidites from north-west to east in the core transect (Fig. 7) demonstrates that the corresponding turbidity currents were generated by the Kander River. The flood-turbidite record and the resulting age-depth model are presented using the example of core THU07-02 (Fig. 12A).

At the core top, Layer A is associated with the 2005 flood event that caused major damage in the Lake Thun area. Layers B and C correlate to severe floods in 1999 and 1968, respectively. Below the organic-rich interval, the thick turbidite of Layer D is associated with a strong flood in 1944. Layer F probably was generated by three consequent flood events in 1930, provoking three successively deposited turbidites. Layer G may represent a catastrophic flood event in 1910, causing only a minor deposit in Lake Thun. Layers J and K could not be correlated with specific floods, but they probably reflect a period with intense flooding between 1860 and 1890. This high flood frequency might be a consequence of the end of the Little Ice Age (LIA) cold period, which was accompanied by high volumes of melt water and sediment from the vanishing glaciers (Pfister, 1988). The outstanding flood turbidite near the base of the gravity short cores (Layers L) correlates to a high-magnitude flood in 1852.

The correlated events were triggered primarily by heavy precipitation, often in combination with snow melt and, less frequently, by thunderstorms (Table 2). Out of this record, the flood events in 2005 and 1852 are among the most extreme floods in Switzerland during the past 160 years (Röthlisberger, 1991; Bundesamt für Wasser und Geologie, 2005c). These floods were caused by similar weather situations with heavy precipitation cells over central Switzerland (Röthlisberger, 1991; Frei, 2005). Both the 1852 and the 2005 flood deposit show, in addition to the coarse-grained base, a second 'pulse' of coarse material (Fig. 8A and B). It is possible that this second pulse reflects a temporal offset between the peak runoffs of the Kander and Simme Rivers (Fig. 1). In 1910, Switzerland was affected by another catastrophic flood event. However, this event did not lead to a notable deposit in Lake Thun; this is certainly due to the different weather situation having the centre of heavy precipitation located in eastern Switzerland, while only minor precipitation cells

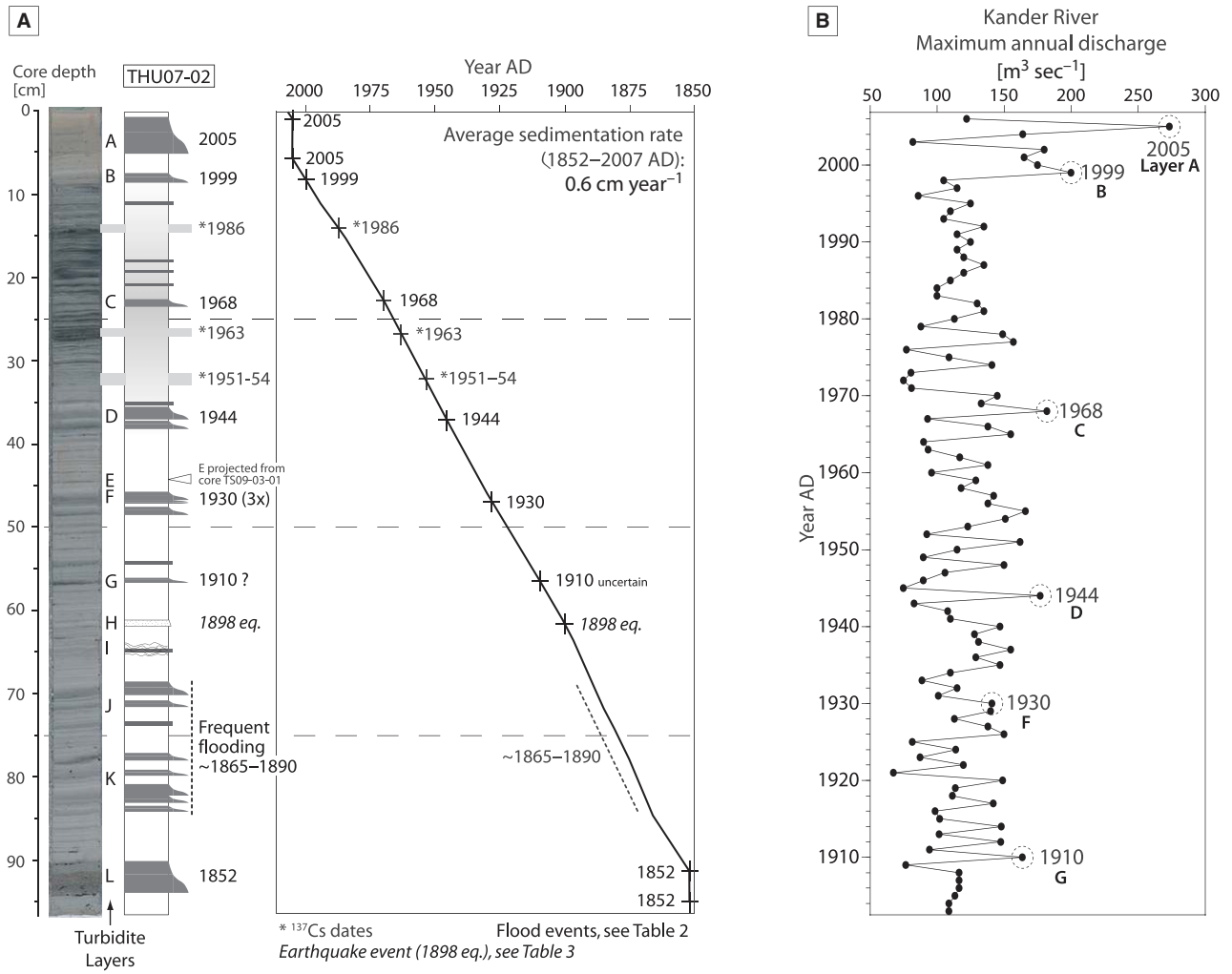

Fig. 12. (A) Correlation of prominent flood turbidites in core THU07-02 to major historically and/or instrumentally documented flood events since 1850 (lithology legend in Fig. 7). As a result, a more detailed age-depth model can be established. (B) Maximal annual discharge of the Kander River between 1903 and 2006 (for location of gauging station, refer to Fig. 1, letter 'B'). Note that most of the highest discharge values correlate to prominent turbidite layers in the sediment record.

were situated over the Lake Thun area (Röthlisberger, 1991; Gilli *et al.*, 2003; Frei, 2005).

The presented flood events were compared with the maximum annual discharge of the Kander River, which has been recorded since 1903 (Fig. 12B, location of gauging station: letter 'B' in Fig. 1; Bundesamt für Umwelt, 1903 to 2007). Except for the deposits related to the three consecutive events in 1930, the presented flood-related turbidites correlate to most of the highest discharge values of the Kander River; this indicates that the size of turbidite deposits is, to a certain extent, dependent on flood magnitude and the associated mobilization of sediment. However, many other factors may influence sediment mobilization and transport during a flood event. For instance, sediments that were mobilized during a strong flood but remained in the catchment may be easily remobilized by a minor flood, thus creating a sediment-storage effect (Gilbert *et al.*, 2006).

Subaquatic mass-movement events since 1714

Seismic data revealed that an increase in mass-movement frequency appeared simultaneously with the Kander River deviation in 1714, raising the question of related trigger mechanisms. Former studies have shown that earthquake-induced shocks play an important role in Swiss lakes (e.g. Monecke *et al.*, 2004; Schnellmann *et al.*, 2006; Strasser *et al.*, 2007). Monecke *et al.* (2004) used sediments from various Swiss lakes to demonstrate that deformation structures start to be

Table 2. Major flood events and their correspondent triggers occurring between 1850 and 2006 and correlating to prominent flood-related turbidite deposits in sediment cores (Figs 7, 8 and 12).

Year	HP	SM	Th	H-M	Layer
2005 August	x			x	A
1999 May	x	x			B
1968 September	x				C
1944 November/ December	x				D
1930 July			x		F
1930 June			x		F
1930 May	x	x			F
1910 June	x	x		x	G
1860 to 1890	x	x			J and K
1852 September	x			x	L

HP, heavy precipitation; SM, snow melting; Th, thunderstorm, H-M, high-magnitude event. Source: Röthlisberger (1991), Bundesamt für Wasser und Geologie (1999); Bundesamt für Wasser und Geologie (2005c).

formed at a groundshaking intensity of VI, and that an even higher intensity of VII and more is necessary to induce basin-wide slope failures.

However, these values may be dependent on the actual conditions in the sediments. The rapid sediment accumulation due to the Kander River deviation probably reduced the threshold for slope failures, especially at the Kander Delta slopes. For the period between 1714 and 2001, seven earthquake events with epicentres within 30 km of Lake Thun are registered in the earthquake catalogue of Switzerland (ECOS, Fäh *et al.*, 2003; Table 3). Moment Magnitudes (M_w) were between 4·2 and 5·6 and intensities (I_0) were between V and VII (Youd, 1973; Fäh *et al.*, 2003; Monecke *et al.*, 2004). In the core record, turbidite deposits of Layers H, M and N can be associated with the earthquakes in Kandersteg (1898), Interlaken (1835) and Wengen (1827), respectively; in contrast, no earthquake events match the coarse deposits of Layers P and Q (Fig. 13A). The stratigraphic position of the events in 1774 and 1729, the latter being one of the strongest earthquakes ever registered in Switzerland, is situated beyond the length of the sediment core record. However, it seems very likely that these events also provoked slope failures; they may be represented by two of the numerous transparent seismic intervals (Fig. 13A).

The crucial factor for earthquake-induced liquefaction is the presence of water-saturated sediment material (Monecke *et al.*, 2004). Water content rapidly decreases with greater core depth, restricting the generation of deformation structures to the immediate vicinity of the sediment surface. Observed deformations occuring within the stratigraphic interval correspond to the time period 1880 to 1900. Hence, the earthquakes potentially responsible for the small-scale deformation structures are the three events in 1881, 1885 and 1898 (Table 3). However, analysis of the exact stratigraphic position of the various deformation structures showed that a correlation of specific deformations to a particular earthquake event is not possible.

Even so, the number of seismically imaged turbidite intervals in the deep lake basin is larger than the number of registered earthquakes potentially responsible for slope failures. Such a deficit of registered events compared with evidence in the sediments is often observed because historic records are lacking low-intensity earthquakes (Rodríguez Pascua *et al.*, 2003). However, in Lake Thun, the Kander River deviation creates an extraordinary situation and this deficit may thus

Table 3. Earthquake events in the Lake Thun area (Fäh *et al.*, 2003) correlating to deposits in the seismic data and/or in the sediment core record from the central deep lake basin.

Year	M_w	I_0	Location	Epicentral distance to Lake Thun (km)	Correlated deposits
1898	4·8	VII	Kandersteg (BE)	*ca* 20	Unit H: Fg-t and Unit I: Def
1885	5	VI	Zweisimmen (BE)	*ca* 30	Unit I: Def
1881	5	VII	Bern (BE)	*ca* 30	Unit I: Def
1835	4·2	V	Interlaken (BE)	*ca* 2	Unit M: Cg-t
1827	4·3	V	Wengen (BE)	*ca* 10	Unit N: Cg-t
1774	5	V	Bern (BE)	*ca* 30	Probably S-t
1729	5·6	VI	Frutigen (BE)	*ca* 10	Probably S-t

See Figs 7 and 13 for stratigraphic position of the correlated deposits.
Fg-t, fine-grained turbidite deposit; Cg-t, coarse-grained turbidite deposit; Def, small-scale deformation structures (Layer I); S-t, transparent turbidite interval in seismic data; M_w, moment magnitude; I_0, intensity.

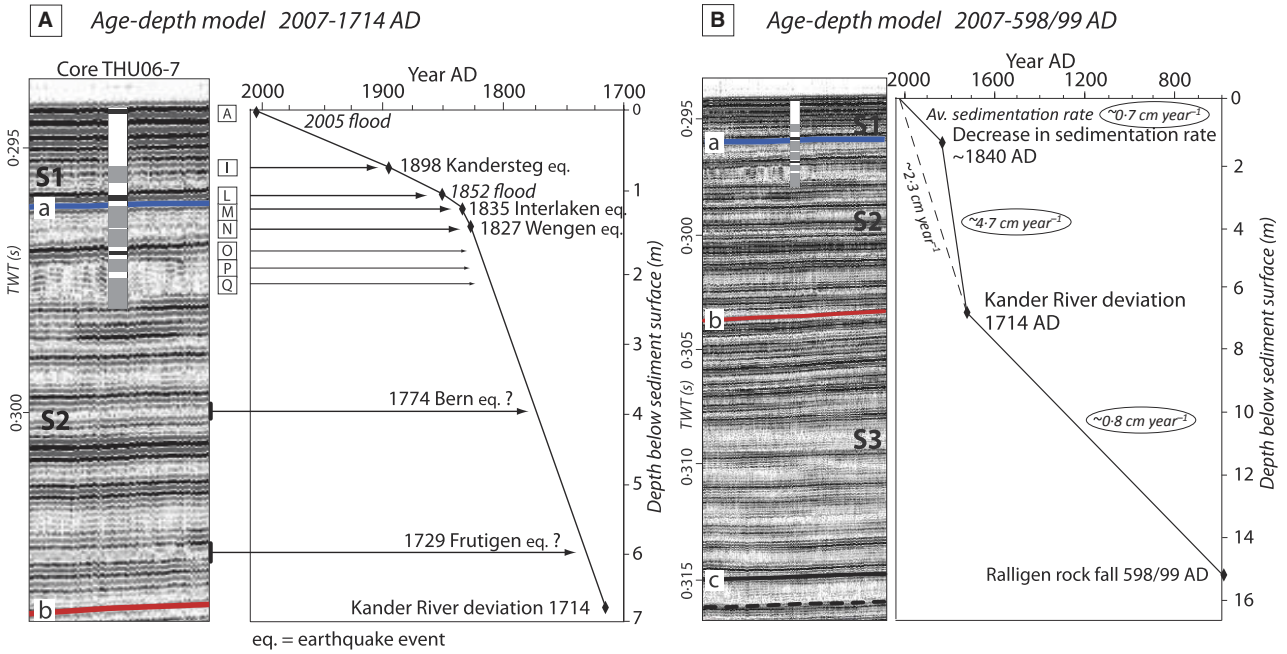

Fig. 13. (A) Age-depth model between 1714 and 2007, based on the event layer record of sediment core THU06-7 and on seismic data in the deep lake basin (for the full seismic profile, see Fig. 4A). Dates for the age-depth model are provided by the Kander River deviation, by three earthquake events in 1827, 1835 and 1898 correlating to mass-movement turbidites in core THU06-7 (Table 3), as well as by two high-magnitude flood events in 1852 and 2005 (Table 2 and Fig. 12A). Layer O (flood) and Layers P and Q (mass movements) do not correlate to any documented events. (B) Age-depth model extended to 598/599 at the same location, based on seismic event horizons defined by the Ralligen rock fall in 598/599, the Kander River deviation in 1714 and the decrease in sedimentation rate *ca* 1840. As a result of the mass-movement-related turbidites, sedimentation rates are very high between 1714 and 1840, whereas they readjust to pre-Kander conditions after 1840.

be explained by additional trigger mechanisms. It is very likely that mass movements were also triggered by other, non-seismic events including: rapid sediment accumulation leading to under-consolidated sediments and pore-fluid overpressure; gas releases due to biochemical processes; and the destabilization of lake-shore sediments by gravel removal and lake-level fluctuations (Gorsline *et al.*, 2000; Nakajiama & Kanai, 2000; Sultan *et al.*, 2004; Girardclos *et al.*, 2007; Strasser & Anselmetti, 2008). In addition, non-seismic trigger mechanisms are likely because the assumption of predominantly earthquake-induced mass movements would imply an enormous increase in seismic activity since 1714 for which no scientific or historic evidence exists.

It is likely that many slope failures in Lake Thun are mostly due to rapid sediment accumulation, as the Kander Delta grew very fast after the Kander River deviation. This rapidly growing load of sediment may have induced pore-fluid overpressures in the underlying low-permeability fine-grained sediments, thus destabilising the entire succession. In addition, short-term water and sediment discharge peaks during flood events of the Kander River, as well as lake-level fluctuations, are very likely to have intensified such unstable conditions on the delta slopes. Highly unstable slope conditions are witnessed not only by the numerous mass flows but also by the general delta-slope morphology with the undulating/hummocky shape of the seismic reflections, interpreted as resulting from sediment creep (Fig. 4B to D, Sequence S1).

VARIATION IN SEDIMENT INPUT

The Kander River deviation induced large changes in sediment input. Sedimentation rates were reconstructed with seismic event data for the pre-Kander period and with both sediment cores and seismic data for the time period after 1714. In addition, sediment yields of the Kander River, as well as erosion rates in the Kander catchment area since 1714, were evaluated by sediment-volume calculations.

Pre-Kander sedimentation rate

Evidence for the pre-Kander sedimentation rate is given through the acoustically masked section on the crossing seismic profile near Spiez (Fig. 5B). This section, interpreted as a mass-movement deposit, is possibly the product of a rock-fall event in the village of Ralligen in 598/599, which is mentioned in a historic report (Fredegarius, 1888). The geographical locations of Ralligen at the lake shore and of the transparent section in the seismic data match perfectly (Fig. 2A). The report also mentions 'dead fish washed ashore' and a 'cooking lake', supporting the hypothesis of a major impact wave affecting the lake shores. Whether the Ralligen rock fall was linked to an earthquake event is unclear, neither the earthquake catalogue of Switzerland (ECOS, Fäh *et al.*, 2003) nor historic documents could give evidence for this possibility.

Using this time horizon, sedimentation rates during seismic Sequence S3 (pre-Kander: 598/599 to 1714) vary between 0·4 and 0·7 cm year^{-1}, depending on the location in the lake basin. For the time period since the Kander River deviation (Sequences S1 + S2, 1714 to 2007), sedimentation rates geographically range from 0·6 to 2·3 cm year^{-1}, thus representing an increase in sediment input by a factor of two or three because of the Kander River deviation. This result is consistent with the doubling or tripling proposed by Sturm & Matter (1972).

Quantification of the Kander River sediment input

Moreover, sedimentation rates have not been constant since the Kander River deviation (Fig. 13). The first 130 years after the river deviation were dominated by intense river channel erosion, high sediment input and instabilities at the Kander Delta slopes indicated by the frequent mass-movement events. Several aspects of the present results point to a subsequent decrease in sediment input and in the frequency of mass-movement events occurring *ca* 1840: (i) the sediment thickness map of seismic Sequence S1 (Fig. 6A) shows a quite uniform lateral distribution of the sediment, in contrast to the uneven sediment distribution during seismic Sequence S2 (Fig. 6B); (ii) large mass-movement deposits are not observed on the slope towards the Kander Delta in seismic Sequence S1, where only evidence of sediment creep is observed (Fig. 4B to D); (iii) mass-movement-related turbidite deposits older than 1840 are coarser and thicker than the turbidites deposited after 1840 (Figs 7 and 8); and (iv) the grain sizes of flood-related deposits become finer, as illustrated by the difference in grain size between the two high-magnitude flood events in 1852 and 2005 (Fig. 8A and B). These observations might reflect reduced sediment input to the lake due to a decline in water energy and sediment availability in the catchment area after 1840. Consequently, a slight stabilization of the lake sediments is observed, particularly in the Kander Delta area.

Sediment yields and erosion rates

The observed reduction in sediment input since 1840 is corroborated by sediment-volume calculations providing sediment yields of the Kander River during seismic Sequences S1 (1852 to 2007) and S2 (1714 to 1852; Table 4). As boundary layers for the volume calculations, the sediment surface as well as seismic Horizons a and b are used (see Fig. 2B for the dimension of the used grid). Although Horizon a is defined in the Kander Delta region, Horizon b can only be extrapolated into the Kander Delta from the slope in the north-western part of the lake because of the acoustic blanking of the delta gravel that was deposited mainly during Sequence S2. To quantify the Kander-derived sediment yield, values for lake-sediment porosity, the fraction of authigenic calcite in the lake sediment and non-Kander

Table 4. Sediment yields of the Kander River and erosion rates in the Kander catchment area for seismic Sequences S1 and S2 derived from lake-sediment volumes, confirming a decrease in sediment input by a factor of 1·9.

	Lake-sediment volume (Mm^3)	Mineral-grain volume (KR) (Mm^3)	Sediment yield (KR) (t km^{-2} year^{-1})	Erosion rate (KR) (mm year^{-1})
Sequence S1 (1852 to 2007 AD, 155 years)	107·7	24·2	363	0·14
Sequence S2 (1714 to 1852 AD, 138 years)	182·5	41·0	690	0·22

Lake-sediment density = 1·5 g cm^{-3}; mineral grain density = 2·6 g cm^{-3}; fraction of authigenic calcite = 20%; non-Kander sediment input = 7·5%; catchment area of Kander River = 1120 km^2.
KR, Kander River.

sediment input are required. Using an average sediment density of 1·5 ± 0·1 g cm^{-3} given by the multi-sensor core logger data and a mineral grain density of 2·6 g cm^{-3}, a porosity of 69 ± 6% was calculated for the lake sediment. Organic content is very low and therefore negligible for the grain density (Fig. 11B). Regarding the authigenic calcite fraction, it is assumed that most of the inorganic carbon in the sediment is bound in calcite, thus indicating a calcite content of *ca* 26% after the Kander River deviation (see Fig. 11B for TIC). Because probably only a small fraction of the carbonate derives from detrital calcite grains (see low-Ca XRF-counts in turbidite layers; Fig. 11B), an authigenic calcite content of 20 ± 5% is assumed. To estimate the amount of the non-Kander sediment input, the value of 15% (Table 1; Sturm & Matter, 1972) is reduced to 7·5 ± 2·5%, as the lake area covered by the applied grid (Fig. 2B) does not contain lateral regions and the eastern platform that are most susceptible to non-Kander sediment input. In general, the calculations provide minimal values because no correction for gravel withdrawal was applied due to a lack of records reliably quantifying these activities. Incorporating the stated uncertainty of the applied parameters, the error of the final yields is estimated to be *ca* 22%.

The resulting sediment yields for the Kander River of 363 and 690 t km^{-2} $year^{-1}$ for seismic Sequences S1 and S2 (Table 4), respectively, confirm a decrease in sediment input by a factor of 1·9. The sediment yield of 363 t km^{-2} $year^{-1}$ is consistent with 200 to 400 t/km^{-2} $year^{-1}$ given by Hinderer (2001) for the modern sediment yield. Furthermore, these sediment yields correspond to erosion rates in the Kander River catchment of 0·14 mm $year^{-1}$ (S1) and 0·22 mm $year^{-1}$ (S2), respectively (Table 4). The erosion rate of 0·14 mm $year^{-1}$ for Sequence S1 agrees with modern denudation rates of 0·15 mm $year^{-1}$ for the total Kander River catchment (Kander River: 0·3 mm $year^{-1}$, Simme River: 0·03 mm $year^{-1}$) derived from measurements of the suspended river load (Schlunegger & Hinderer, 2003). As chemical weathering is not included in the present sediment-yield based calculations, absolute denudation rates increase by the amount of limestone dissolution.

Factors reducing the sediment input

The most important factor contributing to the decrease in sediment input is probably the decline of the erosion in the deviation channel and further upstream in the Kander River bed once the river had adjusted to its new base level. The evaluation of river cross-profiles shows that bed incision has stabilized with <1·5 m level altitude variation between 1970 and 2000 (Tiefbauamt des Kantons Bern and Amt für Landwirtschaft und Natur des Kantons Bern, 2004).

In addition, human activities affecting the catchment area and the lake could also have played an important role:

1 Intense engineering on the Kander River bed between 1899 and 1950 (Eidgenössisches Departement des Innern & Eidgenössisches Oberbauinspektorat, 1890 to 1916; Tiefbauamt des Kantons Bern and Amt für Landwirtschaft und Natur des Kantons Bern, 2004) reduced the energy level and, therefore, the sediment transport capacity of the river. Hence, these corrections contributed to a decrease of transported grain-size ranges and to a general reduction in sediment input.

2 Gravel withdrawal at the Kander Delta since 1913 (Niklaus, 1969; Tiefbauamt des Kantons Bern and Amt für Landwirtschaft und Natur des Kantons Bern, 2004) has diminished the delta volume and probably the chance of slope failures due to reduced overloading of the delta slopes. In addition, gravel withdrawal in the Kander River itself (*ca* 20 km upstream) since 1950 (Tiefbauamt des Kantons Bern and Amt für Landwirtschaft und Natur des Kantons Bern, 2004) has reduced the sediment input to the lake.

3 The installation of water gates at the outflows of Lake Brienz in 1856 (Geiser, 1914) and Lake Thun in the 1870s and 1880s (Vischer, 2003) contributed to a more stable lake level and, therefore, might have stabilized shore and delta sediments.

Relating to climate, the end of the LIA, which is well-documented by the beginning of the retreat of the Grindelwald glacier (Pfister, 1988) *ca* 30 km from Lake Thun, chronologically fits the change in sedimentation rate *ca* 1840. In theory, the end of the LIA should have led to an increased sediment input due to increased melt water and glacial sediment availability. However, this phenomenon is not observed in the present data, perhaps because of the strength of other factors, particularly the initial river adjustments. Nevertheless, the enhanced frequency of flood-related turbidites between 1860 and 1890 (Layers J and K; Fig. 12A) is a possible signature of this climate shift at the end of the 19th Century.

The consequence of the reduced sediment input since *ca* 1840 is more stable lacustrine

sediments, as indicated by the absence of major subaquatic mass-movement deposits. Accordingly, the ammunition material dumped between 1920 and 1963 has probably never been affected by major mass movements. Only slow 'creeping' in the north-western part of the lake and minor fine-grained mass-movement turbidites (Layers E and H) were detected in the seismic and sediment record after 1840. However, results show that a strong magnitude earthquake in the Lake Thun area could trigger subaquatic mass movements involving large sediment volumes, in similar ways as for other peri-alpine lake basins (Schnellmann *et al.*, 2002; Strasser *et al.*, 2007). Thus, such an event represents an important environmental hazard regarding remobilization of ammunition material, as well as potential economic loss linked to the damage of the recently installed gas pipeline.

CONCLUSIONS

The artificial redirection of the Kander River in 1714, which delivered large volumes of sediment into Lake Thun, has led to persistent changes in the sedimentary system of the lake. Sedimentologically, the Kander River deviation is represented by the emergence of large seismic units with a chaotic/transparent facies in the proximity of the Kander Delta. In the distal deep lake basin, the date of the Kander River deviation is defined by the base of a prominent onlap geometry, demonstrating a shift of the depositional centre and confirming a change in direction of the main sediment input from the eastern tributaries to the Kander River. In the sediment core record, the onset of the Kander River input is recorded by an increase in Ca and inorganic carbonate concentrations, reflecting the carbonate-rich catchment area of the Kander River.

Seismic profiles and sediment cores indicate frequent mass-movement events between 1714 and *ca* 1840. The mass movements are very likely to be triggered by failures of the overloaded Kander Delta slopes due to rapid sediment accumulation, lake-level fluctuations and/or earthquake-induced shocks (M_w: 4·2 to 5·6 and I_0: V to VII). Mass-movement deposits are proximally deposited as large units with a chaotic/transparent seismic facies and appear distally as turbidite intervals in the deepest part of the lake.

After 1840, the sediment input to Lake Thun decreased. This reduction is reflected in the absence of major mass-movement deposits, in finer grain sizes of the flood-related turbidite deposits, in a generally more uniform sediment distribution and in a lower sediment yield of the Kander River. The reduction is associated with the adjustment of the Kander River to its new base level, which thus took *ca* 130 years and resulted in less intense river-bed erosion. In addition, human activities, such as lake-level regulations and structural corrections on the Kander River bed, as well as gravel withdrawal in the river bed and at the Kander Delta, have also contributed to the reduction of the sediment loads of the Kander River. However, 'creeping' movements in the north-western lake part and minor mass-movement-related turbidite deposits in the distal deep lake basin still occur.

Flood turbidites that can be followed through the complete core transect correlate to major flood events of the Kander River between 1850 and 2006. This flood-turbidite record includes the events in 1852, 1910, 1930, 1944, 1968, 1999 and 2005. The two thickest turbidites correlate to high-magnitude flood events in 1852 and 2005, ranking among the most severe floods in Switzerland within the past 160 years.

Despite the efforts that were taken for realising the Kander River deviation, this action could not completely solve the flooding problem in the Lake Thun area. The river deviation indeed reduced floods in the further downstream areas of the Kander River but led to higher waters at the lake outflow in the city of Thun. This problem has recently been addressed by the construction of a subterranean high water discharge tunnel at the lake outflow, which is currently in its testing stage. Ongoing management, such as this, of environmental systems that impinge on human activities requires the best possible knowledge base. This study demonstrates the importance of understanding a lake sedimentary or any sedimentary system before realising an extensive engineering project. Valuable knowledge is gained that may make it possible to anticipate positive and negative consequences for the hydrological and sedimentological environment, as well as for economic and societal sectors.

ACKNOWLEDGEMENTS

The authors thank Jonas Zimmermann for assisting in the field and Robert Hofmann for the great technical support. We would also like to thank Adrian Gilli, Fritz Schlunegger and an anonymous reviewer for comments and discussions on

the manuscript. Gabriela Schwarz-Zanetti provided information on historical events in the Lake Thun area. ^{137}Cs activities were measured by Erwin Grieder at Eawag. This research was undertaken as a Masters Thesis at the Limnogeology group of ETH Zurich and as part of the research project on 'Quantifying Holocene clastic sedimentation in peri-alpine lakes' financed by the Swiss National Science Foundation (Grant 620-066113).

REFERENCES

Amt für Gewässerschutz und Abfallwirtschaft des Kantons Bern (2003) *Gewässerbericht 1997–2000*. Bern, 78 pp.

Anselmetti, F.S., Bühler, R., Finger, D., Girardclos, S., Lancini, A., Rellstab, C. and **Sturm, M.** (2007) Effects of Alpine hydropower dams on particle transport and lacustrine sedimentation. *Aquat. Sci.*, **69,** 179–198.

Appleby, P.G. (2001) Chronostratigraphic techniques in recent sediments. In: *Tracking Environmental Change Using Lake Sediments, Volume 1: Basin Analysis, Coring, and Chronological techniques* (Eds W.M. Last and J.P. Smol), pp. 171–203. Kluwer Academic Publishers, Dordrecht.

Arnaud, F., Revel, M., Chapron, E., Desmet, M. and **Tribovillard, N.** (2003) 7200 years or Rhône river flooding activity in Lake Le Bourget, France: a high-resolution sediment record of NW Alps hydrology. *Holocene*, **15,** 420–428.

Beck, C. (2009) Late Quaternary lacustrine paleo-seismic archives in north-western Alps: Examples of earthquake-origin assessment of sedimentary disturbances. *Earth-Sci. Rev.*, **96,** 327–344.

Bernet, D., Liedtke, A., Bittner, D., Eggen, R.I.L., Kipfer, S., Küng, C., Largiader, C.R., Suter, M.J.-F., Wahli, T. and **Segner, H.** (2008) Gonadal malformations in whitefish from Lake Thun: defining the case and evaluating the role of EDCs. *Chimia*, **62,** 383–388.

Bertrand, S., Charlet, F., Chapron, E., Fagel, N. and **De Batist, M.** (2008) Reconstruction of the Holocene seismotectonic activity of the Southern Andes from seismites recorded in Lago Icalma, Chile, 39 degrees S. *Palaeogeogr. Palaeoclimatol. Palaeoecol.*, **259,** 301–322.

Bogdal, C., Naef, M., Schmid, P., Kohler, M., Zennegg, M., Bernet, D., Scheringer, M. and **Hungerbühler, K.** (2009) Unexplained gonad alterations in whitefish (*Coregonus* spp.) from Lake Thun, Switzerland: levels of persistent organic pollutants in different morphs. *Chemosphere*, **74,** 343–440.

Bundesamt für Umwelt (1903 to 2007) Hydrological data - Discharge of Kander, Simme and Aare Rivers. Annual maximal discharge 1903-2006: station 1117 Kander-Hondrich. Discharge August 2005 in 10 minute intervals: stations 488 Simme-Latterbach, 2469 Kander-Hondrich. Daily average discharge 2007: stations 488 Simme-Latterbach, 2030 Aare-Thun, 2457 Aare-Ringgenberg, 2469 Kander-Hondrich. Bern.

Bundesamt für Wasser und Geologie (1999) *Hochwasser 1999 – Analyse der Ereignisse*. Bern, 6 pp.

Bundesamt für Wasser und Geologie (2005a) *Geologische Karte der Schweiz, 1:500'*000. Bern.

Bundesamt für Wasser und Geologie (2005b) *Tektonische Karte der Schweiz, 1:500'*000. Bern.

Bundesamt für Wasser und Geologie (2005c) *Bericht über die Hochwasserereignisse 2005*. Bern, 25 pp.

Chapron, E., Beck, C., Pourchet, M. and **Deconinck, J.-F.** (1999) 1822 earthquake-triggered homogenite in Lake Le Bourget (NW Alps). *Terra Nova*, **11,** 86–92.

Eidgenössisches Departement des Innern & Eidgenössisches Oberbauinspektorat (1890 to 1916) *Die Wildbachverbauung in der Schweiz/nach ausgeführten Werken, Heft 1, 2 und 4*. Stämpfli'sche Buchdruckerei, Bern.

Eidgenössisches Departement für Verteidigung, Bevölkerungsschutz und Sport (2004) Historische Abklärungen zu Ablagerungen und Munitionsversenkungen in Schweizer Seen, Zusammenfassung. Bern, 8 pp.

Erdgas Thunersee AG (2009) Erdgas Thunersee AG, Available at: http://www.erdgasthunersee.ch (Last accessed: 17 February 2011).

Fäh, D., Giardini, D., Bay, F., Bernardi, F., Braunmiller, J., Deichmann, N., Furrer, M., Gantner, L., Gisler, M., Isenegger, D., Jimenez, M.J., Kästli, P., Koglin, R., Masciadri, V., Rutz, M., Scheidegger, C., Schibler, R., Schorlemmer, D., Schwarz-Zanetti, G., Steimen, S., Sellami, S., Wiemer, S. and **Wössner, J.** (2003) Earthquake Catalogue Of Switzerland (ECOS) and the related macroseismic database. *Eclogae Geol. Helv.*, **96,** 219–236.

Fredegarius (1888) Chronicarum quae dicuntur Fredegarii scholastici, Liber IV. In: *Monumenta Germaniae Historica (MGH)* (Ed. B. Krusch), *Script. Rer. Mer.*, 128 pp.

Frei, C. (2005) *August-Hochwasser 2005: Analyse der Niederschlagsverteilung*. MeteoSchweiz, Zürich.

Froitzheim, N., Plašienka, D. and **Schuster, R.** (2008) Alpine tectonics of the Alps and Western Carpathians. In: *The Geology of Central Europe, Volume 2: Mesozoic and Cenozoic* (Ed. T. McCann), pp. 1141–1233. The Geological Society, London.

Gaillard, M.-J., Dearing, J.-A., El-Daoushy, F., Enell, M. and Håkansson, H. (1991) A late Holocene record of land-use history, soil erosion, lake trophy and lake-level fluctuations at Bjäresjösjön (South, Sweden). *J. Paleolimnol.*, **6,** 51–81.

Geiser, K. (1914) *Brienzersee und Thunersee: Historisches und Rechtliches über den Abfluss*. Buchdruckerei Rösch & Schatzmann, Bern, 174 pp.

Gilbert, R., Crookshanks, S., Hodder, K.R., Spagnol, J. and **Stull, R.B.** (2006) The record of an extreme flood in the sediments of montane Lillooet Lake, British Columbia: implications for paleoenvironmental assessment. *J. Paleolimnol.*, **35,** 737–745.

Gilli, A., Anselmetti, F.S., Ariztegui, D. and **McKenzie, J.A.** (2003) A 600-year sedimentary record of flood events from two sub-alpine lakes (Schwendiseen, Northeastern Switzerland). *Eclogae Geol. Helv.*, **96**(Suppl. 1), 49–58.

Gilli, A., Anselmetti, F.S., Glur, L. and **Wirth, S.B.** (in press) Lake sediments as archives of recurrence rates and intensities of past flood events. In: *Tracking Torrential Processes on Fans and Cones* (Eds M. Bollschweiler, M. Stoffel and F. Rudolf-Miklau), *Springer Ser. Adv. Global Change Res.*

Girardclos, S., Schmid, O.T., Sturm, M., Ariztegui, D., Pugin, A. and **Anselmetti, F.S.** (2007) The 1996 delta collapse and large turbidite in Lake Brienz. *Mar. Geol.*, **241,** 137–154.

Gorsline, D.S., De Diego, T. and **Nava-Sanchez, E.H.** (2000) Seismically triggered turbidites in small margin basins: Alfonso Basin, Western Gulf of California and Santa Monica Basin, California Borderland. *Sed. Geol.*, **135,** 21–35.

Hieke, W. (2000) Transparent layers in seismic reflection records from the cental Ionian Sea (Mediterranean) – evidence for repeated catastrophic turbidite sedimentation during the Quaternary. *Sed. Geol.*, **135,** 89–98.

Hinderer, M. (2001) Late Quaternary denudation of the Alps, valley and lake fillings and modern river loads. *Geodin. Acta*, **14,** 231–263.

Kastens, K.A. and **Cita, M.B.** (1981) Tsunami-induced sediment transport in the abyssal Mediterranean Sea. *Geol. Soc. Am. Bull., Part I*, **92,** 845–857.

Matter, A., Süsstrunk, A.E., Hinz, K. and **Sturm, M.** (1971) Ergebnisse reflexionsseismischer Untersuchungen im Thunersee. *Eclogae Geol. Helv.*, **64,** 505–520.

Monecke, K., Anselmetti, F.S., Becker, A., Sturm, M. and **Giardini, D.** (2004) The record of historic earthquakes in lake sediments of Central Switzerland. *Tectonophysics*, **394,** 21–40.

Moreno, A., Valero-Garcés, B.L., González-Sampériz, P. and **Rico, M.** (2008) Flood response to rainfall variability during the last 2000 years inferred from the Taravilla Lake record (Central Iberian Range, Spain). *J. Paleolimnol.*, **40,** 943–961.

Mueller, A.D., Islebe, G.A., Anselmetti, F.S., Ariztegui, D., Brenner, M., Hodell, D.A., Hajdas, I., Hamann, Y., Haug, G.H. and **Kennett, D.J.** (2010) Recovery of the forest ecosystem in the tropical lowlands of northern Guatemala after disintegration of Classic Maya polities. *Geology*, **38,** 523–526.

Mulder, T. and **Alexander, J.** (2001) The physical character of subaqueous sedimentary density flows and their deposits. *Sedimentology*, **48,** 269–299.

Mulder, T., Syvitski, J.P.M., Migeon, S., Faugères, J.-C. and **Savoye, B.** (2003) Marine hyperpycnal flows: initiation, behavior and related deposits. A review. *Mar. Petrol. Geol.*, **20,** 861–882.

Nakajiama, T. and **Kanai, Y.** (2000) Sedimentary features of seismoturbidites triggered by the 1983 and older historical earthquakes in the eastern margin of the Japan Sea. *Sed. Geol.*, **135,** 1–19.

Nast, M. (2006) *Überflutet – überlebt – überlistet: Die Geschichte der Juragewässerkorrektionen*. Verein Schlossmuseum Nidau, Nidau, 192 pp.

Niklaus, M. (1969) *Die Kander und ihr Delta im Thunersee*. Jahrbuch vom Thuner- und Brienzersee, Interlaken, pp. 59–85.

Noren, A.J., Bierman, P.R., Steig, E.J., Lini, A. and **Southon, J.** (2002) Millenial-scale storminess variability in the northeastern United States during the Holocene epoch. *Nature*, **419,** 821–824.

Obermeier, S.F. (1996) Use of liquefaction-induced features for paleoseismic analysis – an overview of how seismic liquefaction features can be distinguished from other features and how their regional distribution and properties of source sediment can be used to infer the location and strength of Holocene paleo-earthquakes. *Eng. Geol.*, **44,** 1–76.

Pfister, C. (1988) *Klimageschichte der Schweiz 1525–1860: das Klima der Schweiz von 1525–1860 und seine Bedeutung in der Geschichte von Bevölkerung und Landwirtschaft, Band I*. Verlag Paul Haupt, Bern, 225 pp.

Rayleigh, L. (1885) On waves propagated along the plane surface of an elastic solid. *Proc. Lond. Math. Soc.*, **17,** 4–11.

Rellstab, C., Keller, B., Girardclos, S., Anselmetti, F.S. and **Spaak, P.** (2011) Anthropogenic eutrophication shapes the past and present taxonomic composition of hybridizing *Daphnia* in unproductive lakes. *Limnol. Oceanogr.*, **56,** 292–302.

Richter, T.O., van der Gaast, S., Koster, B., Vaars, A., Gieles, R., de Stigter, H.C., de Haas, H. and **van Weering, T.C.E.** (2006) The Avaatech XRF Core Scanner: technical description and applications to NE Atlantic sediments. In: *New Techniques in Sediment Core Analysis* (Ed. R.G. Rothwell), *Geol. Soc. London Spec. Publ.*, **267,** 39–50.

Rodríguez Pascua, M.A., De Vicente, G., Calvo, J.P. and **Pérez-López, R.** (2003) Similarities between recent seismic activity and paleoseismites during the late Miocene in the external Betic Chain (Spain): relationship by 'b' value and the fractal dimension. *J. Struct. Geol.*, **25,** 749–763.

Röthlisberger, G. (1991) *Chronik der Unwetterschäden in der Schweiz*. Berichte der Eidg. Forschungsanstalt für Wald, Schnee und Landschaft, 330, Birmensdorf, 122 pp.

Rothwell, R.G., Hoogakker, B., Thomson, J., Croudace, I.W. and **Frenz, M.** (2006) Turbidite emplacement on the southern Balearic Abyssal Plain (western Mediterranean Sea) during Marine Isotope Stages 1-3: an application of ITRAX XRF scanning of sediment cores to lithostratigraphic analysis. In: *New Techniques in Sediment Core Analysis* (Ed. R.G. Rothwell), *Geol. Soc. London Spec. Publ.*, **267,** 79–98.

Schlunegger, F. and **Hinderer, M.** (2003) Pleistocene/Holocene climate change, re-establishment of fluvial drainage network and increase in relief in the Swiss Alps. *Terra Nova*, **15,** 88–95.

Schnellmann, M., Anselmetti, F.S., Giardini, D., McKenzie, J.A. and **Ward, S.N.** (2002) Prehistoric earthquake history revealed by lacustrine slump deposits. *Geology*, **30,** 1131–1134.

Schnellmann, M., Anselmetti, F.S., Giardini, D. and **McKenzie, J.A.** (2006) 15,000 Years of mass-movement history in Lake Lucerne: implications for seismic and tsunami hazards. *Eclogae Geol. Helv.*, **99,** 409–428.

Shiki, T., Kumon, F., Inouchi, Y., Kontani, Y., Sakamoto, T., Tateishi, M., Matsubara, H. and **Fukuyama, K.** (2000) Sedimentary features of the seismo-turbidites, Lake Biwa, Japan. *Sed. Geol.*, **135,** 37–50.

Siegenthaler, C. and **Sturm, M.** (1991) Die Häufigkeit von Ablagerungen extremer Reuss-Hochwasser. Die Sedimentationsgeschichte im Urnersee seit dem Mittelalter. *Mitt. Bundesamt f. Wasserwirtschaft*, **4,** 127–139.

Siegenthaler, C., Finger, W., Kelts, K. and **Wang, S.** (1987) Earthquake and seiche deposits in Lake Lucerne, Switzerland. *Eclogae Geol. Helv.*, **80,** 241–260.

Steiner, A. (1953) Die Zuschüttung des Thunersees. *Geogr. Helv.*, **8,** 226–233.

St-Onge, G., Mulder, T., Piper, D.J.W., Hillaire-Marcel, C. and **Stoner, J.S.** (2004) Earthquake and flood-induced turbidites in the Saguenay Fjord (Québec): a Holocene paleoseismicity record. *Quatern. Sci. Rev.*, **23,** 283–294.

Strasser, M. and **Anselmetti, F.S.** (2008) Mass-movement event stratigraphy in Lake Zurich: a record of varying seismic and environmental impacts. In: *Quantifying Late Quaternary Natural Hazards in Swiss Lakes: Subaquatic Landslides, Slope Stability Assessments, Paleoseismic Reconstructions and Lake Outbursts* (Ed. Schweizerische Geotechnische Kommission (SGTK)), *Beiträge zur Geol. der Schweiz, Geotechn. Serie*, No. 95, 23–41. Zürich.

Strasser, M., Stegmann, S., Bussmann, F., Anselmetti, F.S., Rick, B. and **Kopf, A.** (2007) Quantifying subaqueous slope stability during seismic shaking: Lake Lucerne as model for ocean margins. *Mar. Geol.*, **240,** 77–97.

Sturm, M. and **Matter, A.** (1972) Sedimente und Sedimentationsvorgänge im Thunersee. *Eclogae Geol. Helv.*, **65,** 563–590.

Sultan, N., Cochonat, P., Canals, M., Cattaneo, A., Dennielou, B., Haflidason, H., Laberg, J.S., Long, D., Mienert, J., Trincardi, F., Urgeles, R., Vorren, T.O. and **Wilson, C.** (2004) Triggering mechanisms of slope instability processes and sediment failures on continental margins: a geotechnical approach. *Mar. Geol.*, **213,** 291–312.

Tiefbauamt des Kantons Bern and Amt für Landwirtschaft und Natur des Kantons Bern (2004) *Geschiebehaushalt Kander*. Hunziker, Zarn & Partner, Aarau, 59 pp.

Vischer, D.L. (2003) Die Geschichte des Hochwasserschutzes in der Schweiz. *Berichte des BWG, Serie Wasser*, Nr. 5, 61–70. Bern.

Weltje, G.J. and **Tjallingii, R.** (2008) Calibration of XRF core scanners for quantitative geochemical logging of sediment cores: theory and application. *Earth Planet. Sci. Lett.*, **274,** 423–438.

Wirth, S. (2008) *Lake Thun sediment record: 300 years of human impact, flood events and subaquatic slides*. MSc thesis, Department of Earth Sciences, ETH Zürich. Available at: http://e-collection.ethbib.ethz.ch/view/eth:30790.

Youd, T.L. (1973) Liquefaction, flow, and associated ground failure. *US Geol. Surv. Circular*, **688,** 12.

Manuscript received 7 July 2010; revision accepted 3 February 2011